ABSTRACT

Imaging in ophthalmology has considerably improved over the past years, but only selected techniques allow high resolution imaging of the anterior segment.

Many studies have been published on investigations of the posterior segment of the eye. Recently these studies can also be an useful in examining the anterior segment of the eye at microscopic resolution. It can be helpful to image and measure complex details of corneal pathologies and structural changes of the chamber angle and the iris, as found in Optical Coherence Tomography.

Key Words:

Corneal topography, imaging techniques, OCT, UBM, slit lamp.

Introduction

Imaging in ophthalmology has considerably improved over the past years, but only selected techniques allow high resolution imaging of the anterior segment (Wilkins et al.,1996).

With understanding the principles of the anterior segment imaging , through examination techniques, and knowledge of imaging characteristics of a variety of intraocular pathologies, different imaging techniques of the eye are vital part of an ophthalmologist's diagnostic. Without these tools, the clinician may not be able to detect or manage a variety of ocular diseases (Byrne et al., 1992) .

From the imaging techniques of the anterior segment which was providing high resolution, two-dimensional imaging of the anterior segment. Recently by using three-dimensional imaging as in Ultrasound Biomicroscopy which is useful in elucidating the anatomic correlates of a wide variety of disorders, including anterior segment tumors, angle-closure glaucoma, malignant glaucoma, pigment dispersion syndrome, trauma, and inflammatory diseases (Woo et al.,1999).

Many studies have been published on investigations of the posterior segment of the eye. Recently these studies can also be an useful in examining the anterior segment of the eye at microscopic resolution. It can be helpful to image and measure complex details of corneal pathologies and structural changes of the chamber angle and the iris, as found in Optical Coherence Tomography (Fujimoto et al., 1995).

New method of measuring and quantifying the shape and the curvature of the corneal surface using Corneal topography. Most topographers consist of a placido disc made up of multiple circles, which is backlit or projected onto the corneal surface. The resultant circular images are reflected and captured with a video camera and digitized (Joo et al.,1999).

Aim of work:

To evaluate the various imaging techniques for investigating anterior segment diseases using corneal topography, biometry, ultrasound biomicroscopy.

Slit Lamp Photography

Introduction:

The slit lamp is a special microscope that provides a magnified, three-dimensional view of the different parts of the eye. A slit lamp examination is done to look at the anterior segment of the eye, including the cornea, lens, iris, and the front section of the vitreous gel. Special lenses can be placed between the slit lamp and the cornea (or directly on the cornea) to view deeper structures of the eye, such as the optic nerve and the area where fluid drains out of the eye (drainage angle). A camera may be attached to the slit lamp to take photographs of different parts of the eye (Kattie et al., 2003).

Instrumentation:

Assessment of the anterior segment is performed using a slit lamp video imaging system. The entire system consists of a slit lamp with a video camera attached, a fiber optic background illuminator, a personal computer with a video capture card, image management software, and a foot pedal switch for capturing digital still images. All of the major slit lamp manufacturers make camera ready slit lamps. There are several functional parameters that need to be considered when configuring a slit-lamp video imaging system. First, it is important to note that a background illumination source is a must, because the native lighting of the slit-lamp is attenuated by beam splitters and thus, does not provide sufficient illumination to provide good quality images(Kattie et al., 2003).

Secondly, it is important to determine whether the system you are purchasing has parafocal or nonparafocal optics. With parafocal systems, the attached camera will achieve a focused image in the same plane as the optics of the slit lamp. With nonparafocal systems, the attached camera does not achieve a focused image in the same plane as the optics of the slit lamp and therefore, requires that the examiner look at the computer monitor during the image capture process. Parafocal optics is ideal because of ease of use, but is more costly. Lastly, one needs to keep in mind that the ability to perceive depth is significantly reduced, because the images are two-dimensional representations of a three dimensional structure. Moreover, very fine detail, such as cell and flare is impossible to detect with current video imaging systems (Kattie et al., 2003).

A cost-effective alternative to the slit-lamp video imaging systems is a slit-lamp digital still camera photographic system. Only one such system has been described to date (Adam et al.,2003).

The digital still camera slit lamp system described consists of a 950 or 990 digital camera, a 10X eyepiece, and a standard Haag Streit slit lamp. The eyepiece adapter is screwed directly onto the digital camera, and the other end of the eyepiece is inserted directly into one of the slit lamp eyepiece ports (Adam et al.,2003).

The digital camera is set at ISO 100, no flash, and focus at infinity, with the white balance set according to the illumination on a piece of white paper placed in front of the slit lamp. The camera point of focus does not always align with the slit lamp light source and thus, the slit lamp beam may need to be tilted in order to achieve proper illumination. High-resolution still images can be obtained and readily transferred to a computer via the serial or USB port. No video capture card is necessary (Adam et al.,2003).

The slit lamp examination can be viewed in real-time using the slit lamp video imaging system described above. To accomplish real-time viewing of the slit lamp exam, the video output from the camera must be sent through the CODEC (compressor/decompressor) of the videoconferencing system being used. This is achieved by attaching the video output cable from the camera to the video input port of the CODEC (Daniel et al.,2003).

Alternatively, if the camera is being used generates both a composite and S-video signal, then simultaneous delivery of the video signal to the two different input devices can be achieved by sending the composite signal to one device and the S-video signal to the other device. S-video is of higher quality than composite (Daniel et al.,2003).

Because transmission of real-time video through a CODEC requires signal compression, the quality of the real-time video is significantly degraded and does not provide adequate resolution to make in-depth clinical inferences. Therefore, real-time slit lamp video assessments must be coupled with high-resolution digital still images in order to be clinically useful. Because of the reduced image quality, real-time slit lamp video assessments are generally used to guide the remote site examiners to the areas of suspected pathology in order to capture a digital still for more detailed review (Daniel et al.,2003).

Other aspects of the anterior segment examination that need to be addressed technically as intraocular pressure measurements and corneal topography. Intraocular pressure measurements can be performed using traditional slit lamp-based Goldmann applanation, assuming appropriately trained personnel are present at the remote site (Kattie et al., 2003).

Hand-held tonometers are ideal for telemedicine applications, because they require minimal training and provide accurate and reproducible measurements. Remotely following refractive surgery patients can be done with the use of a slit lamp video imaging system in conjunction with a corneal topography unit that exports the topographic files in one of the standard file formats (Kattie et al., 2003).

A wide variety of corneal and anterior segment photographs will be showed in figures. Darrel L. Conger, CRA October 2000.

(figure 1) A wide variety of corneal and anterior segment photographs taken using a photographic version of the slit lamp. Darrel L. Conger, CRA October 2000.

(a) Intraocular Lens

(b) Traumatic Aniridia

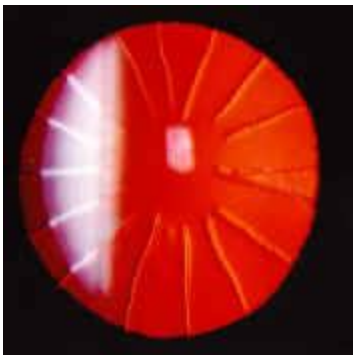

(c) 16 Cut RK

(d) Inter Corneal Blood

(e)Laser Bubbles

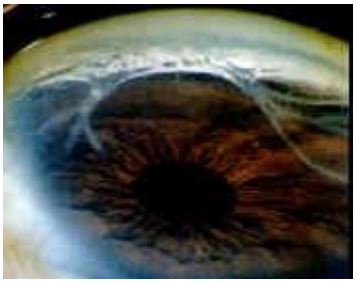

(f) Parinaud's Oculo-Grandular Syndrome

(g) Corneal Deposits

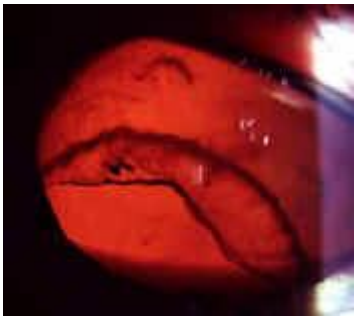

(h) Dislocated Crystalline Lens

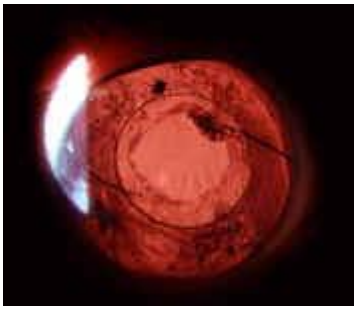

(i) IOL S/P Yag Capsulotomy

(j) Silicon Oil Bubbles In AC

(k) Iris Tumor

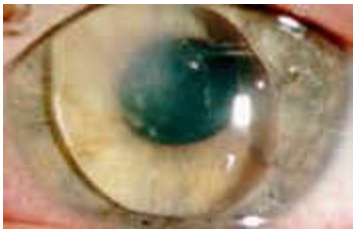

(l) Crystalline Lens In AC

(m) IOL Sticking Through PK

(n) Expulsed Retina

(o) Diffraction Of Light Through Edematous Cornea

(p) Acanthamoeba Keratitis

Corneal Topography

Introduction:

Imaging techniques of the cornea are developing rapidly, mainly because of recent advances in refractive surgery. To understand the significance of new imaging techniques, the relevant principles of corneal optics are reviewed. The discussion of the most common clinical method of Placido-based corneal topography emphasizes important concepts of its clinical interpretation (Peter et al.,2005).

Corneal topography is a method of measuring and quantifying the shape and the curvature of the corneal surface. Most topographers consist of a placido disc made up of multiple circles, which is backlit or projected onto the corneal surface. The resultant circular images are reflected and captured with a video camera and digitized (Joo et al.,1999).

Corneal Optics And Structure:

Different concepts are used to characterize optical properties of the cornea.

- Curvature of its anterior and posterior surface can be expressed as radii of curvature in millimeters or clinically more often in keratometric diopters.
- The shape of the anterior and posterior surface also can be expressed in micrometers as the elevation of the actual surface relative to a chosen reference surface (e.g. sphere). These 2 concepts can characterize the overall shape and the macro-irregularities of the corneal surface (e.g. corneal astigmatism).
- Local surface changes can be expressed in micrometers. Smoothness of the surface is optically very important, and any micro-irregularities of the corneal surface can significantly degrade the image.
- Power of the cornea expressed as refraction in diopters is an optical property dependent on the shape of the surfaces and the refractive index of the surface.
- Thickness and 3-D structure of the cornea can be expressed in micrometers. Changes in the 3-D structure (e.g. after refractive surgery) can induce further changes of its shape because of

biomechanical changes, such as altered elasticity of the remaining tissue.

This concept is a simplification ignoring the fact that the refracting surface is air-tear interface, and it does not account for the oblique incidence of incoming light in the corneal periphery. As a result, it miscalculates a true corneal refractive index of 1.376 to 1.3375 to correct for some of these factors. That is why these diopters more correctly are termed keratometric diopters to distinguish them from the diopters expressing more precisely the true refractive power at certain corneal point (Holladay et al., 1997).

Corneal Shape:

The average anterior and posterior corneal power is 48.6 diopter (D) and– 6.8 D, respectively. To simplify it in clinical practice or in keratometry, a substitution with one refractive surface with the resulting corneal power of 42-44 keratometric D often is used. The average cornea changes little with age. It flattens about 0.5 D by age 30 years and steepness about 1 D by age 70 years (Naufal et al., 1997).

During adulthood, an average cornea is steeper in the vertical meridian by about 0.5 D compared to the horizontal meridian, which contributes to higher incidence of with the rule astigmatism in young adults. This difference between vertical and horizontal curvature diminishes with age, finally disappearing at age 70 years. Lenticular changes contribute significantly to the higher incidence of against the rule astigmatism with age (Edmund et al., 1994).

Normal cornea is a prolate surface, i.e. steeper in the center and flatter in the periphery. Oblate surface (e.g. surface after myopic laser photorefractive keratectomy) is flatter in the center and steeper in the periphery (Kaufman et al., 2000).

The visually significant area of the corneal surface is approximately the area with the same diameter as the pupil size. The pupil diameter decreases with age. A large variation exists between people in any age group. In one large study, the average pupil size in individuals aged 20 and 80 years was 4.5 mm and 3.5 mm, respectively, in bright illumination (Kaufman et al., 2000).

In dim illumination, the average pupil size in individuals aged 20 and 80 years was 8 mm and 5 mm, respectively. This finding is clinically important because most refractive lasers treat an area with a 6.5-mm diameter with a surrounding blending zone (Wilson et al., 1991).

Corneal topography instruments used in clinical practice most often are based on Placido reflective image analysis. This method of imaging of the anterior corneal surface uses the analysis of reflected images of multiple concentric rings projected on the cornea (Belin et al., 1992)

Corneal Topography – Principles:

Multiple light concentric rings are projected on the cornea. The reflected image is captured on charge-coupled device (CCD) camera. Computer software analyzes the data and displays the results in a variety of formats (Krachmer et al., 1997).

Interpretation Of Topographic Maps:

Every map has a color scale that assigns particular color to certain keratometric dioptric range. Never base an interpretation on color alone. The value in keratometric D is crucial in the clinical interpretation of the map and has to be looked at with the interpretation of every map (Petroll et al., 1996).

Absolute maps have a preset color scale with the same dioptric steps, dioptric minimum and maximum assigned to the same colors for particular instrument. These maps allow direct comparison of 2 different maps. Although, because the steps are in large increments (generally 0.5 D), their disadvantage is that they do not show subtle changes of curvature and can miss subtle local changes (e.g. early keratoconus) (Hitzenberger et al., 1994).

Normalized maps have different color scales assigned to each map based on the instrument software that identifies the actual minimal and maximal keratometric dioptric value of a particular cornea. The dioptric range assigned to each color generally is smaller compared to the absolute map, and, consequently, maps show more detailed description of the surface. The disadvantage is that the colors of 2 different maps cannot be compared directly and have to be interpreted based on the keratometric values from their different color scales (Petroll et al., 1996).

Using the mathematics of convex mirrors and proprietary mathematical algorithms, the image size is measured and quantified. The resulting data are displayed as a corneal curvature map. The maps consist of colors corresponding to corneal power and curvature; steep contours are displayed as warm colors (e.g. red), while flat contours correspond to cool colors (e.g. green, blue) (Kezirian et al., 1999).

Corneal Topography Measurements:

Corneal topography most commonly is thought of as Placido-based reflective image analysis. It does not directly measure the x, y, and z coordinates of the points on the corneal surface that usually are used for characterization of objects in 3-D space. Instead, it typically measures the deviation of reflected rings and primarily calculates the curvature of the corneal surface points in axial direction (Liu et al.,1999).

Curvature/Power Map:

Surface curvature measures how fast the surface bends at a certain point in a certain direction.

Axial curvature (formerly termed sagittal curvature) measures the curvature at a certain point on the corneal surface in axial direction relative to the center. It requires the calculation of the center of the image, which cannot be measured directly (Herndon et al.,1997).

Meridional curvature (formerly termed tangential and instantaneous curvature) measures the curvature at a certain point on the corneal surface in meridional direction relative to the other points on the particular ring (Herndon et al.,1997).

Meridional curvature maps always are more sensitive measures of local curvature change. Axial curvature maps can be derived from meridional maps. Axial value at a certain point equals the average meridional curvature along the radius from the map center to the point of interest, thereby approximating the average refractive power (Herndon et al.,1997).

Axial and meridional maps should be displayed theoretically in the units of radii of curvature (i.e. mm) at each corneal surface point. For ophthalmologists who better understand more clinically used units of D in ophthalmic practice, the instruments display curvature in units of

keratometric D and constitute so-called axial or meridional power maps (Liu et al.,1999).

Elevation Map:

Elevation is not measured directly by Placido-based topographers, but certain assumptions allow the construction of elevation maps. Elevation of a point on the corneal surface displays the height of the point on the corneal surface relative to a spherical reference surface (Peter et al., 2005).

The reference surface in most instruments was chosen to be a sphere. Best mathematical approximation of the actual corneal surface called best-fit sphere is calculated by instrument software for every elevation map separately. The same surface may appear different when mapped against different reference surfaces. Consequently, it is difficult to compare directly 2 elevation maps that likely have slightly different best-fit spheres as reference values, and comparison only can be intuitive (Peter et al., 2005).

Notice that in practice the colors in the same region of elevation and axial curvature maps often are reversed. The vertical 90° axis is steeper in those incidences of with the rule corneal astigmatism. Therefore, the superior area typically is depressed (blue on elevation map and steeper, red on axial map) (Bogan et al., 1990).

The bow tie pattern on the axial map is just a different mathematical representation of an oval spherocylindrical surface. It is not seen on the elevation map that is created from the x, y, and z coordinates of the usual representation of data in a 3-D world (Salz et al., 1983).

Interpretation Of Topographic Indices:

Simulated K (SimK): Simulated keratometry measurements characterize corneal curvatures in the central 3-mm area. The steep simulated K-reading is the steepest meridian of the cornea, using only the points along the central pupil area with 3-mm diameter (Holladay et al., 1997).

The flat simulated K-reading is the flattest meridian of the cornea and is by definition 90° apart. These readings give an idea about the central corneal curvature that is frequently visually most significant. The 3-mm diameter was chosen primarily from historical reasons for the purpose of comparison

with standard keratometry that is used for analysis of 4 central points, 3.2 mm apart (Lemp et al., 1985).

The index of asphericity: The index of asphericity indicates how much the curvature changes upon movement from the center to the periphery of the cornea. A normal cornea is prolate (i.e. becomes flatter toward the periphery) and has the asphericity Q of -0.26. A prolate surface has negative Q values and positive oblate surface values. Most myopic laser vision corrections change the anterior corneal surface from prolate to oblate (Bogan et al., 1990).

Indices characterizing the uniformity and optical quality of the anterior corneal surface: Currently, best spherocylindrical correction that is used in glasses, soft contact lenses, and laser vision correction and are reflected in keratometric indices do not correct all the optical aberrations of the corneal surface .The best visual acuity also requires uniform smooth anterior corneal surface (Petroll et al., 1996).

A variety of these indices try to relate the variability of the actual values of the anterior corneal surface obtained by corneal topography to the optical quality and potential best visual acuity that would be permitted by the anterior corneal surface (Peter et al.,2005).

These indices can be thought of in clinical practice as different mathematical estimates of the visual disturbance that can be expected to be caused by the amount of irregularities of the anterior corneal surface. Many indices specific for each instrument exist. Examples include the following: *surface regularity index (SRI), corneal uniformity index (CUI), predicted corneal acuity (PCA), and point spread function (PSF).* It also is important to realize that patients with normal corneal indices can have poor vision caused by disturbances in any other part of the optical system of the eye (Yaylali et al.,1997).

Limitations of corneal topography: The error of corneal topography is under optimal conditions in the range of ±0.25 D or 2-3 μm, but, in those abnormal corneas seen in clinical practice, it often is ±0.50-1.00 D due to several limitations (Binder et al.,1995).

The imaging requires an intact epithelial surface and tear film. Some of the errors of the Placido-based systems are as follows: focusing errors, alignment and fixation errors with induced astigmatism, difficulty to

calculate the position of the center from the small central rings, increased inaccuracy toward the periphery because the accuracy of each point depends on the accuracy of all preceding points, and other errors (Kaufman et al., 2000).

Different technologies use different measurement methods and algorithms; thus, the output data are not directly comparable. Also, the technologies undergo constant modifications, and the results of studies comparing the instruments are outdated quickly and difficult to interpret for practical clinical purposes (Rabbetts et al.,1998)

In addition, normal spherocylindrical surface imaging techniques should be able to characterize a variety of more complex optical surfaces, as follows: very steep or flat corneas, keratoconus with local steepening, sharp transition zones after uncomplicated refractive surgeries, diffusely irregular surfaces after penetrating keratoplasty, complex surfaces after complicated refractive surgeries with decentered ablations, and central islands. These optical surfaces are more difficult to measure (Herndon et al.,1997)

Corneal Topography In Normal Corneas:

The normal cornea flattens progressively from the center to the periphery by 2-4 D, with the nasal area flattening more than the temporal area. The topographic patterns of the 2 corneas of an individual often show mirror-image symmetry, and small variations in patterns are unique for the individual. The approximate distribution of keratographic patterns described in normal eyes includes the following: round (23%), oval (21%), symmetric bow tie typical for regular astigmatism (18%), asymmetric bow tie (32%), and irregular (7%).

Raster Photography Topography Method:

The posterior apical radius (PAR) imaging device projects a regular pattern of lines or grid of known geometry onto the anterior corneal surface that is viewed from an offset angle. The topical fluorescein is used to stain the tear film, and cobalt blue light is used to illuminate the pattern. The accuracy and reproducibility is in the range of Placido-based systems, but the advantage is that the PAR system does not require an intact epithelial surface (Wilson et al.,1991).

Slit Scan Imaging:

The Orbscan corneal topography system uses a scanning optical slit design that is fundamentally different from the corneal topography that analyzes the reflected images from the anterior corneal surface. The high-resolution video camera captures 40 light slits at the 45° angle projected through the cornea similarly as seen during slit lamp examination (Auffarth et al., 1997).

The instrument's software analyzes 240 data points per slit and calculates the corneal thickness and posterior surface of the entire cornea. The anterior surface of the cornea initially was calculated in this manner; however, since the calculation from the reflected images used by corneal topography is more precise, the current version of Orbscan is using the latter method and is a combination of reflective corneal topography and optical slit design (Yaylali et al., 1997).

Orbscan is the most common instrument in clinical practice that allows the analysis of the corneal thickness and posterior surface of the entire cornea and has the ability to detect abnormalities in those areas. Currently, limited knowledge of the 3-D structure and the mechanical behavior of the cornea, especially after different types of refractive procedures, are available. More detailed knowledge of this behavior could improve the outcomes of refractive procedures (Wilson et al.,1991).

Using the Orbscan corneal topography system software, the standard location of central and periphery cornea can be designed according to clinical requirements. The relative accuracy and precision of the Orbscan system is similar to ultrasonic pachymetry, although measurements of the corneal thickness with the Orbscan system were 23-28 µm greater than those obtained by ultrasonic pachymetry. Preoperative pachymetric measurements of central corneal thickness made with an ultrasonic pachymeter in the PERK study were 20 µm thinner than the measurements made with the Orbscan instrument (Yaylali et al.,1997).

Therefore, the pachymetric measurements by the Orbscan instrument cannot be used interchangeably with ultrasonic pachymetry measurements. One possible explanation for the observed differences in corneal thickness with these two methods is that the Orbscan system is a non-contact method whereas ultrasonic pachymetry requires corneal contact. Another possibility

is that the Orbscan system may also measure the hydrated mucous gel covering the corneal surface that has been reported to be up to 40 μm thick. Despite these discrepancies, the Orbscan corneal topography system appears to offer clinical utility for assessing corneal shape and thickness (Yaylali et al.,1997).

With the interpretation of the abnormalities of the posterior surface of the cornea, it is important to realize that the posterior corneal surface contributes 7 times less compared to the anterior surface to the refractive power of the cornea. The refractive clinical significance of the abnormalities of the posterior surface currently is being investigated (Rabbetts et al.,1998).

The accuracy and repeatability of the instrument is reported to be below 10 μm and, under optimal conditions, in the range of 4 μm in the central cornea and 7 μm in the peripheral cornea. In clinical practice, it is even more dependent than corneal topography on many factors, such as the limited movement of the patient's eye, ability of patients to keep the eye wide open, optically clear cornea, and the presence of corneal abnormalities. The other limitations of current optical slit technology are the inability to detect interfaces (eg after LASIK flap) and the longer time of image acquisition and processing compared to standard Placido-based topography (Rabbetts et al.,1998).

Traditionally, power maps (actually surface curvature) have been axis-centered, which are method dependent and only show one selected piece of the complete angle-dependent power. The new mean and toric decomposition of the complete curvature tensor, allow clinicians for the first time to see and quantify local curvature (and paraxial power) variations as well as the fundamental spherocylindrical components. Full corneal pachymetry allows surgeons to use regional blade settings, to measure the laser ablation depth from a fixed surface (the posterior cornea), and to assess the effect of the posterior surface on corneal power. Accurate knowledge of both surfaces will provide researchers with real data for corneal mechanics simulations. The point of minimum corneal thickness is a local center of axisymmetry, which for normal corneas aligns closely to the overall optical axis of the eye (Carr et al.,2000).

Use Of Corneal Topography In Refractive Surgery:

One of the most promising and exciting developments in the world of refractive surgery has been the advent of laser in situ keratomileusis (LASIK). The surgical technique involves the creation of a hinged lamellar corneal flap, after which an excimer laser is used to make a refractive cut on the underlying stromal bed. LASIK is a fusion of old and new technologies, with its roots in keratomileusis and automated lamellar keratectomy (ALK). However, as currently practiced, it is perhaps best thought of as photorefractive keratectomy (PRK) performed under a flap instead of on the corneal surface (Carr et al.,2000).

Many factors can affect the accuracy and reproducibility of corneal topography maps; these factors include quality of the tear film, the ability of the patient to maintain fixation, and operator experience (Knorz et al., 1998).

Corneal topography is used primarily as a screening tool to evaluate prospective refractive surgery candidates and a diagnostic aid in evaluating refractive surgery patients with poor outcomes. Irregular corneas are poor candidates for refractive surgery since results with current lasers can be unpredictable. Keratoconus and contact lens warpage are the most common causes of irregular corneas in the screening population (Koffler et al., 1991).

Steep (i.e. red) areas isolated to the inferior cornea suggest keratoconus, and many topographers come equipped with programs to alert the clinician when a diagnosis of keratoconus is likely. Postoperative patients with poor vision should have topography; such problems as central islands, irregular ablation profiles, and decentered laser ablations can be assessed with these devices (Koffler et al., 1991).

Corneal topography is essential to rule out keratoconus and irregular astigmatism. These problems tend to make the surgical outcome unpredictable. In particular, keratoconus patients may be more prone to the development of ectasia or thinning following LASIK. Corneal topography also is helpful in evaluating contact lens-induced corneal warping. Patients with irregular corneas and a history of contact lens wear should be observed with serial refractions and topography until both stabilize (Probst et al., 1999).

Follow-Up Lasik Care:

Follow-up examinations are performed on day 1, week 1-2, 3 months, 6 months, and 1 year after surgery. Corneal topography is a useful adjunct in assessing postoperative results and planning enhancements and should be performed several times between week 1 and month 6. Centration and ablation pattern can be assessed best with topography; it is especially useful in patients who have an unexplained decrease in best-corrected visual acuity (Wang et al., 1999).

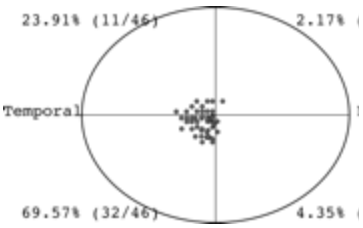

(figure 2) Location of the thinnest site on the cornea measured by the Orbscan corneal topography system.
Fowler CW, Dave TN. Review of past and present techniques of measuring corneal topography. *Ophthalmic Physiol Opt* 1994.

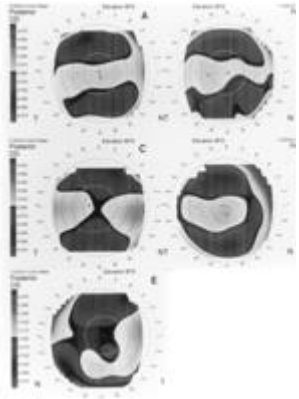

(figure 3) Elevation patterns of the posterior corneal surface: (A) regular ridge; (B) irregular ridge; (C) incomplete ridge; (D) island; (E) unclassified.
Naufal SC, Hess JS, Friedlander MH, *et al*. Rasterstereography-based classification of normal corneas. *J Cataract Refract Surg* 1997.

(figure 4) ORBSCAN II provides anterior segment data in the form of topographic surfaces.

From Idaho eye center 2001.

Idaho Eye Center

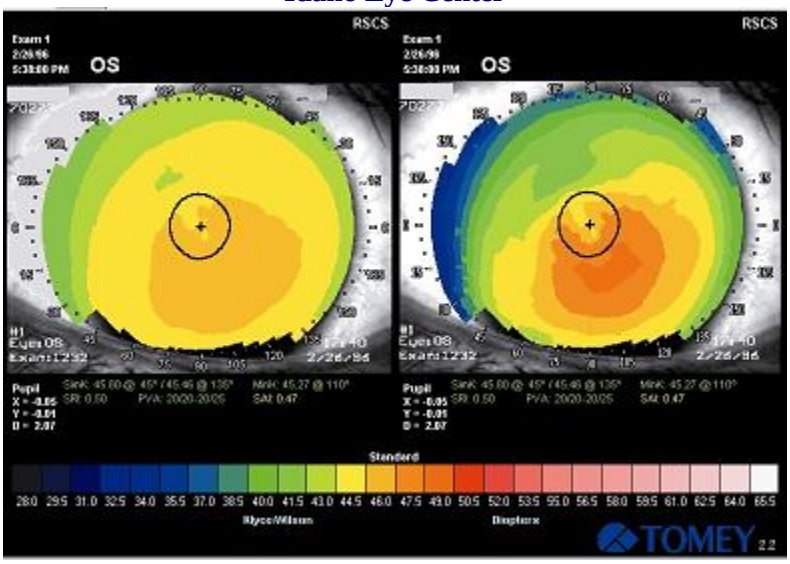

(figure 5) A normal cornea with a slight amount of asymmetry is shown in the left panel using the fixed standard "Klyce/Wilson" scale. Using a self-adapting scale that is built into most corneal topographers, makes this corneal topography look abnormally steep (right panel).
Belin MW, Litoff D, Strods SJ, *et al*. The PAR technology corneal topography system. *Refract Corneal Surg* 1992.

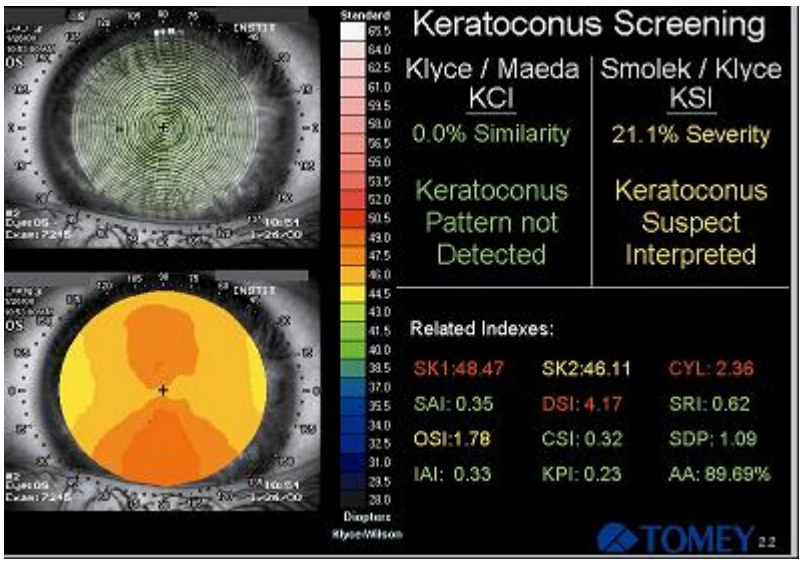

(figure 6) This keratoconus screening program from the Tomey TMS-3 topographer provides two analysis methods..
Yaylali V, Kaufman SC, Thompson HW. Corneal thickness measurements with the Orbscan topography system and ultrasonic pachymetry. *J Cataract Refract Surg* 1997.

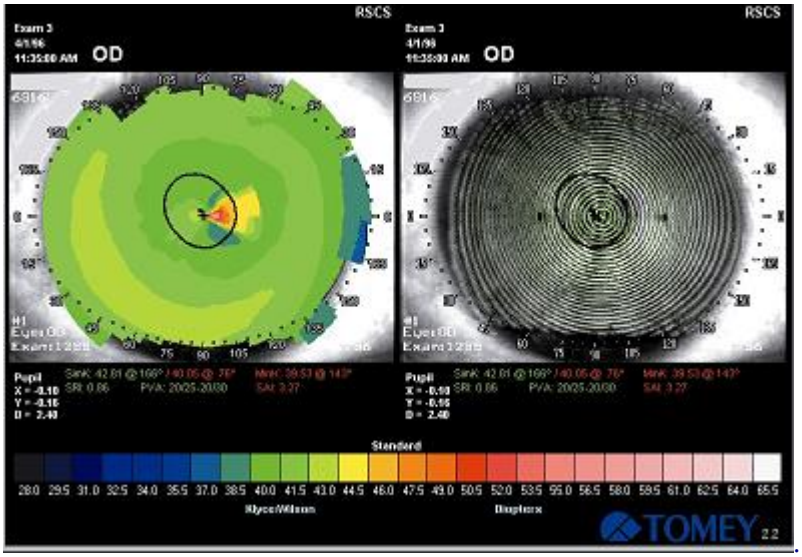

(figure 7) inspection of the mire tracking (right panel) shows that the apparent central irregular astigmatism in the color map (left panel) is due to a mistracking artifact. This was probably due to eye movement during the exam. Edmund C. Posterior corneal curvature and its influence on corneal dioptric power. *Acta Ophthalmol (Copenh)* 1994.

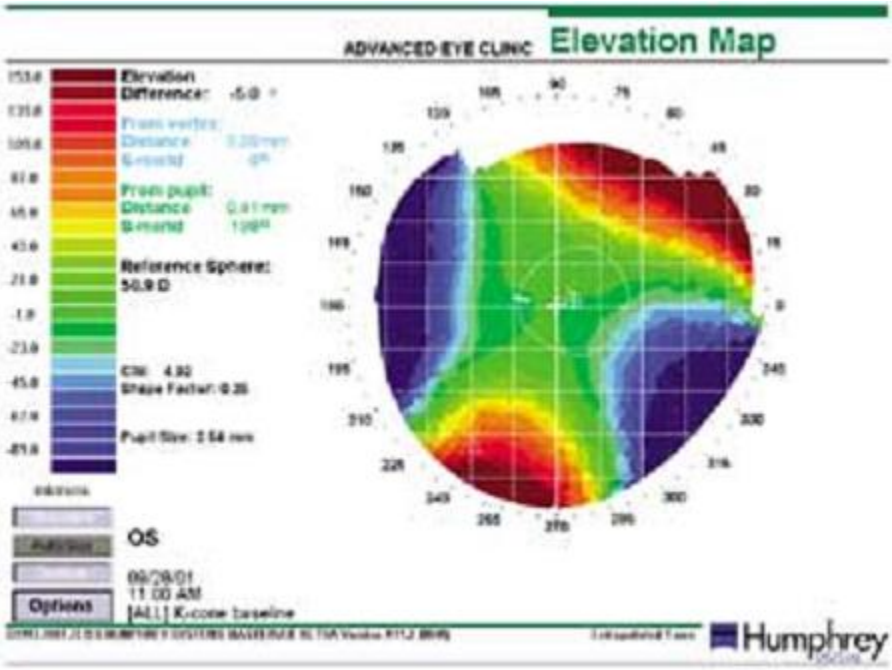

(figure 8) This elevation map shows inferior thinning in a patient's left eye. Yaylali V, Kaufman SC, Thompson HW. Corneal thickness measurements with the Orbscan topography system and ultrasonic pachymetry. *J Cataract Refract Surg* 1997.

Specular Microscopy

Introduction:

Specular microscopy is a photographic test used to visualize the human endothelium. The endothelium is the last layer of cells that make up the cornea. This single cell layer is responsible for both supplying nutrients to the rest of the cornea which has no blood supply and removing debris and waste from the cornea. The cells are about 3000 cells per square millimeter. The cells do not regrow or replace themselves. Instead they grow larger to fill gaps of missing or dead cells. When the cell count falls below a certain amount the cornea can no longer remain clear and healthy. This is often the reason a cornea transplant is performed (Kawana et al., 2004).

Uses Of Specular Microscopy:

There are 2 types of specular microscopy: contact and non contact microscopy.

- non-contact specular microscopy is used to observe endothelial blebs occurring with different types of contact lenses

  Contact lenses induce short- and long-term corneal endothelial changes, including endothelial blebs. The endothelial bleb is a reversible, short-term response found on the corneal endothelium after lens wear (Ohya et al., 1996).

- The new noncontact specular microscope provides measurements of corneal thickness that are somewhat less than those of ultrasound pachymetry, but that seem to be more consistent from one operator to another, possibly as a result of the elimination of observer bias induced by probe placement required by the ultrasound unit. This consistency may be important in the comparison of measurements by different operators over time in patients being followed up after refractive surgery or other therapeutic interventions (Renee et al., 1999).

- To determine endothelial cell density, contact and noncontact specular microscopy may be used interchangeably. However, for the combined measurement of endothelial cell density and pachymetry, the use of the

same specular microscope is recommended for long-term patient follow-up (Laszlo et al.,2002).

Prior to the development of clinical specular microscopy it was believed that the only healing mechanism for the adult human corneal endothelium was the "sloughing and sliding" mechanism whereby damaged endothelial cells sloughed from the endothelium and the adjacent undamaged, or less damaged, cells moved laterally so as to cover the defect left by the sloughed cells. Specular microscopy revealed two additional healing mechanisms. Endothelial cell coalescence (cell fusion), is a mechanism in which the common cell membrane between two cells degenerates to result in a larger cell containing two nuclei and, presumably, all of the cellular organelles of the two individual cells (Neubauer et al.,1983).

Endothelial cell mitosis, once generally believed to be impossible for adult human endothelial cells, has also been demonstrated in the adult human cornea following successful treatment for graft rejection (Laing et al.,1984).

Clinical Application Of Specular Microscopy:

Fuch's Dystrophy

Cornea guttate, characteristic for Fuch's endothelial dystrophy, are focal accumulations of collagen on the posterior surface of Descemet's membrane that apparently are formed by stressed or abnormal endothelial cells; they appear as warts or excrescences of Descemet's membrane and can easily be seen with specular microscopy (Laing et al., 1981).

Lattice Corneal Dystrophy:

Specular microscopy of patients having Lattice Corneal Dystrophy, an autosomal dominant disease, has shown the presence of linear structures described as branching lines criss-crossing the stroma that are believed to be amaloid deposits or lesions caused by amyloid deposition as well as a craterform appearance. Although histologically there are irregularities in the epithelium and in Bowman's zone, no endothelial involvement has been noticed (Takahashi et al., 1987).

Iridocorneal Endothelial Syndrome:

The iridocorneal endothelial syndrome(ICE syndrome), believed to be due to a defect of the corneal endothelium, includes progressive essential iris atrophy, Chandler's syndrome, and the iris nevus (Cogan-Reese) syndrome (Hirst et al., 1983).

An early report of the specular microscopic appearance of the corneal endothelium in Chandler's syndrome described grossly abnormal cells and suggested that the changes could be confused with cornea guttatae. However, a subsequent study indicated that this similarity in specular microscopic findings might be problematic only in advanced cases of the iridocorneal endothelial syndrome and Fuchs' dystrophy, and that the abnormalities observed in the former entity were rather distinctive (Hetherington et al., 1978).

In minimally affected corneas the clinical specular microscopic appearance of the endothelium is characterized as a "rounding-up" of the endothelial cells. There was a loss of cellular definition and hexagonal shape, and many pentagonal cells were evident. There is also an increased granularity of the intracellular details, and small, centric dark areas appear in individual cells. These changes seem to affect virtually all cells (Hirst et al.,1980).

Posterior Polymorphous Dystrophy:

The clinical manifestations of posterior polymorphous dystrophy are similar to those of iridocorneal endothelial syndrome so that the diagnosis is complicated. Many of the features of iridocorneal endothelial dystrophy have been reported in cases of posterior polymorphous dystrophy (Laganowski et al., 1991).

Posterior polymorphous dystrophy is generally regarded to be an inherited, often bilateral abnormality of the posterior, non-banded layer of Descemet's membrane, that may be the result of an abnormality of the corneal endothelium at the time of birth. Unlike iridocorneal endothelial dystrophy, posterior polymorphous dystrophy is generally non-progressive and only occasionally associated with corneal decompensation or glaucoma (Brooks et al., 1989).

Two dystrophies can generally be distinguished by specular microscopy . The dark structures seen in posterior polymorphous dystrophy have a thick dark border and lie anterior to recognizable endothelial cells that have an undistorted appearance and are almost always larger than normal, while the dark structures seen in iridocorneal endothelial dystrophy have a thin dark edge and lie within the endothelium. The endothelial cells adjacent to the dark structure have a distorted appearance and are commonly smaller than normal (Presberg et al.,1986).

Keratoconus:

Specular microscopy of keratoconic corneas has demonstrated the presence of endothelial abnormalities. There appears to be an increase in cellular pleomorphism, a finding that is particularly unusual in view of the relative youth of the population studied. Many cells considerably smaller than normal are distributed throughout the endothelial population (Laing et al., 1979).

Indeed, after clinically scanning photomicrographs the investigators were left with the distinct impression that there are two populations of cells, one larger and the other considerably smaller than normal. The most striking abnormality in keratoconus is directional enlargement of many endothelial cells. The long axis of these cells seems oriented toward the apex of the cone, and the cells themselves appear to have been stretched by the ectatic process (Jakus et al., 1962).

This observation is consistent with the current concept of acute corneal hydrops, wherein stretching of the endothelium and Descemet's membrane is presumed to result ultimately in the rupture of both structures, allowing aqueous humor to enter the corneal stroma. Specular photographs also reveal that many endothelial cells contain a dark structure, which in all instances is completely contained within the cell (Skuta et al., 1983).

Invariably there is a normal-appearing area between the dark structure and the cell boundary, and the latter is normal. These intracellular dark structures seem to occur less frequently in larger endothelial cells. They are consistent in appearance with blebs or

vacuoles seen with the electron microscope, but their role in the pathogenesis of keratoconus is not understood (Laganowski et al.,1991).

In most cases of acute ectasia of the cornea (or corneal hydrops) dehydration of the cornea ultimately occurs. It is presumed that with time the endothelial cells adjacent to the area of rupture enlarge, fill in the defect, and ultimately effect regeneration of Descemet's membrane (Laganowski et al.,1991).

Penetrating Keratoplasty:

Specular microscopy on successful corneal grafts indicate that substantial endothelial cell loss occurs during or immediately after surgery. In many instances there also may be a progressive and sustained cell loss for a considerable period thereafter. Although there is a critical endothelial cell density below which corneal deturgescence cannot be maintained and irreversible edema occurs, early specular microscopy studies showed that a surprisingly low endothelial cell density can maintain the cornea in a dehydrated, transparent state (Sturrock et al.,1978).

Endothelial changes resulting from or occurring after penetrating keratoplasty also have been studied, although it is apparent that such studies are limited to successful, transparent corneal grafts. Giant endothelial cells, indicating extensive cell loss, have been observed while in other instances little or no endothelial cell loss is seen (Abbott et al., 1979).

The variability in endothelial cell loss is great, ranging from 5 to 80% following penetrating keratoplasty. Because a grafted cornea can remain transparent and support 20/20 vision with less than 20 percent of its normal endothelial cell density, specular microscopy is needed to accurately distinguish between a clear corneal transplant with extensive cell loss and one with virtually no cell loss (Bourne et al., 1976).

The specular microscopic data on corneal grafts in patients having ketatoconus who showed evidence of a severe allograft rejection episode revealed a significantly decreased endothelial cell density as

compared to similar patients that showed no evidence of an allograft rejection (Musch et al.,1991).

Specular microscopy has been proven to be of value in following high risk patients since early evidence of graft rejection can be seen. During rejection episodes one sees intercellular bright bodies and black inflammatory cells and generally recognizable keratic precipitates on the endothelial surface. Although adult human endothelial cells do not normally undergo mitosis, this has been reported in a 35 year old grafted cornea that rejected but that was successfully treated with corticosteroid (Ruusuvaara et al., 1980).

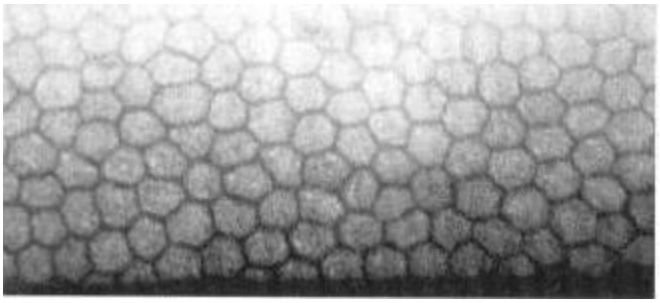

(figure 9).Normal corneal endothelium as photographed by specular microscopy. A quasi-regular array of hexagonal cells all having nearly the same area is seen Hoffer K, Kraft M. Normal endothelial cell count range. *Ophthalmology*. 1980;87:861.

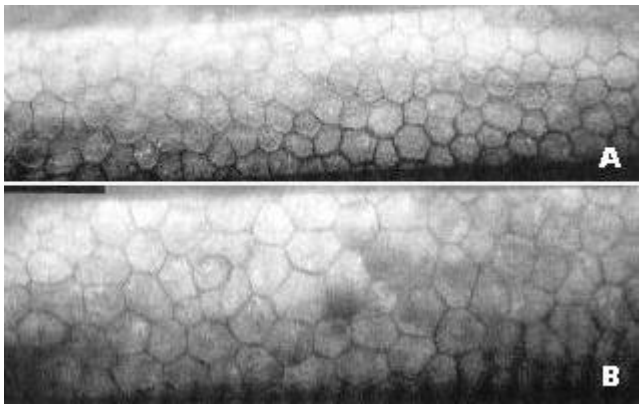

(figure 10).A, Specular microscopic image of corneal endothelium B, Specular microscopic image of the corneal endothelium after anterior chamber IOL implantation.

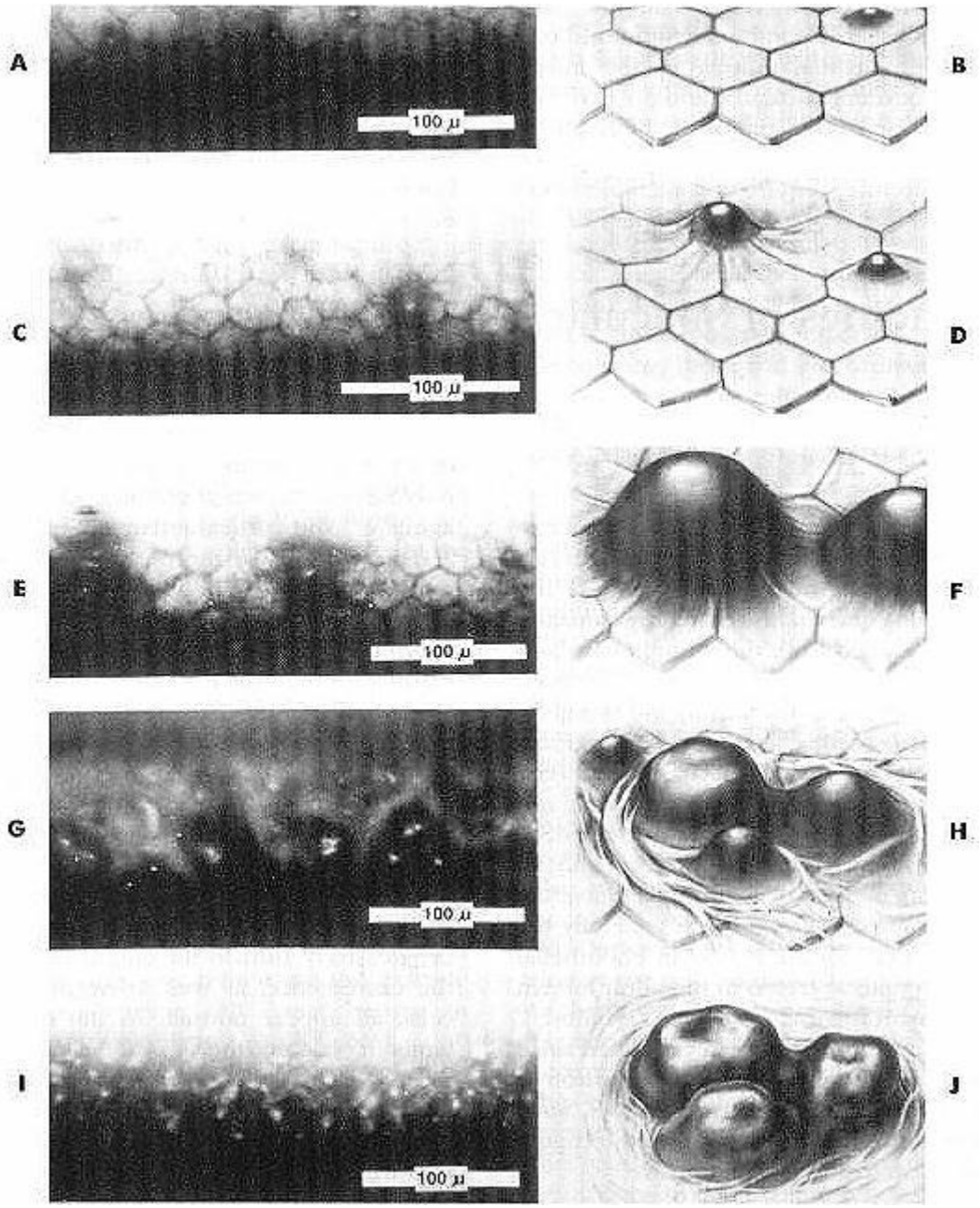

(figure 11).Specular photomicrographs and drawings of various stages of cornea guttata in Fuchs' dystrophy (x 100). A and B, Stage 1: Early form of cornea guttata. Excrescences are smaller than individual endothelial cells. Dark areas are the sides of the excrescence. Bright spots are each a reflex from the apex of the excrescence. C and D, Stage 2: Cornea guttata approximate the average endothelial cell in size. E and F, Stage 3: Cornea guttata are considerably larger than the average endothelial cell. Adjacent endothelial cells are abnormal in appearance. G and H, Stage 4: Individual cornea guttata have coalesced and contain more than one apical bright spot. Boundaries of adjacent endothelial cells are absent or difficult to identify. I and J, Stage 5: Coalesced excrescences and nearly complete disorganization of adjacent endothelial mosaic. Numerous bright structures presumably are collagenous material deposited at the level of Descemet's membrane or on the posterior corneal surface.Laing R, Leibowitz H, Chang R, Theodore J, Oak S. The endothelial mosaic in Fuchs dystrophy. A qualitative evaluation with specular microscope. *Arch Ophthalmol*. 1981;99:80.

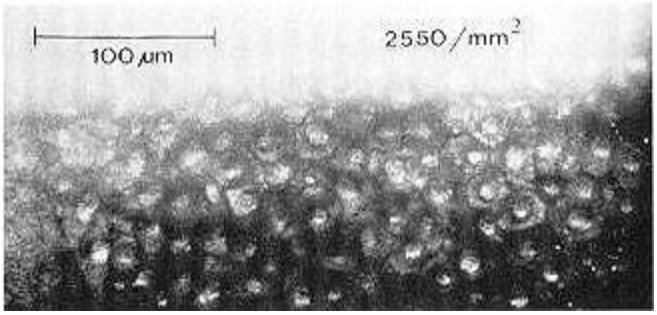

(figure 12).Specular microscopic changes in posterior polymorphous dystrophy. Note the large dark structures. Sherrard E, Novakovic P, Speedwell L. Age-related changes of the corneal endothelium and stroma as seen in vivo by specular microscop y. *Eye*. 1987;1:197.

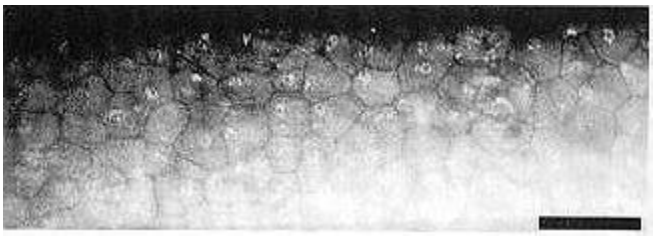

(figure 13).Specular microscopic image of corneal endothelium in rejection. Note the small particles adherent to the endothelium, presumably inflammatory cells. Sherrard E, Novakovic P, Speedwell L. Age-related changes of the corneal endothelium and stroma as seen in vivo by specular microscop y. *Eye*. 1987;1:197.

Fluorophotometry

Most ocular media and tissues are like the dermis in being exposed to electromagnetic radiation on a life long scale. However dermis is continuously renewed, in contrast some ocular media are not and carry for life a trace of the history of their light exposure. A series of photochemical and photobiological events occur within these media, in particular within the crystalline lens and the retina resulting in a permanent modification of their optical and functional properties. Most of these events result in the formation of fluorescent molecular aggregates due to alteration of initially non fluorescent molecules or to accumulation processes. These fluorophores are termed endogenous fluorophores. Their amount and distribution within the eye is related to age and to light exposure and may be modified by pathology (Docchio et al., 1988).

The eye being a multicompartment organ ; biochemical interaction with the external world mainly occur through the blood aqueous barrier located in the anterior segment of the eye. Liquids and molecules may also diffuse into the anterior chamber through the cornea. Fluorescent tracers may be intentionally or unintentionally induced into the eye through this barrier (Docchio et al., 1988).

Endogenous Fluorophores:

The two main endogenous fluorophores are the lens and retinal pigment epithelium (R.P.E.). Other structures such as the cornea, the aqueous and the vitreous body exhibit some degree of fluorescence. However they play a minor role in relation to the diagnosis of ocular diseases due to the higher regeneration rate with respect to the lens and retina (Fagerholm et al., 1981).

Crystalline Lens:

The crystalline lens is basically composed of a solution of protein aggregates termed alpha, beta and gamma crystallines. Most of these crystallines are water soluble and exhibit typical tryptophan fluorescence. The distribution of tryptophan fluorescence is fairly uniform throughout the lens cross section. In contrast, non tryptophan fluorescence is uniform across the optical axis, decreasing from the outmost layers to the nucleus with axial symmetry (Jacobs et al., 1981).

Exogenous Fluorophores:

The most important fluorophore among exogenous fluorophores is sodium fluorescein, which is a dye of the xanthine group used in "Fluorophotometric Techniques". For vitreous fluorophotometry fluorescein is injected I.V., while for anterior segment fluorophotometry, fluorescein is administered topically in the form of eye drops or it may be also injected I.V.. At alkaline ph. it has been shown that the molar intensity of fluorescence of fluorescein is 54 times greater than fluorescein glucuronide. It was shown that the pH of aqueous humour fluorescein is 34 times more fluorescent than fluorescein glucuronide (Chen et al., 1985).

These measurements are made at the excitation peak for fluorescein. If the excitation wave length is varied, the relative molar fluorescent intensity ratio between the two compounds changes dramatically. At 455 nm the intensity of fluorescence of fluorescein is only five times that of fluorescein glucuronide. The relative intensity of fluorescence of these two compounds was calculated by the clinical fluorophotometer. With this instrument, the ratio of intensity between fluorescein and fluorescein glucuronide is 9.7:1 (Chen et al., 1985).

The pharmacokinetics of intravenously and orally administered fluorescein suggests that the dominant fluorophore in the anterior chamber or in the vitreous at first is fluorescein. Many hours after administration of a dose, the molar ratio of these two fluorophores in the eye can only be guessed as their relative contribution to the observed fluorescence intensity (Palestine et al., 1981).

Instrumentation And Techniques

From the above considerations on the accumulation and dynamics of endogenous and exogenous fluorophores in the eye globe, the role of techniques able to monitor these fluorophores directly in the eye is evident. The effectiveness of ocular Fluorophotometric Techniques is based on the ability to couple excitation light of suitable wavelength to the target and to detect fluorescent emission from the target area in a sensitive and selective way (Harding et al.,1981).

***The Major Aspects To Be Considered In Relation To Ocular Fluorophotometry Are*:**

1- Geometry and refractive properties of the ocular bulb:

The eye is an optical device, who's refractive properties have to be taken into consideration in the design of optics to excite ocular fluorophores especially those located close to the retina.

2- Absorption and fluorescence of the optical media:

The eye is a complex system consisting of different compartments all exhibiting absorption and scattering of light at both the excitation and emission wavelengths and most of which are fluorescent.

3- Eye movements:

For these techniques that require a long measuring time eye movements may be critical.

Slit Lamp Fluorophotometry (Imaging Ocular Fluorometry):

The most popular imaging ocular fluorometry techniques are based on modification of standard slit lamp photographic techniques.With a slit lamp fluorophotometric technique is limited to anterior segment to monitor corneal and lens fluorescence (Mayor et al.,1985).

Scheimpflug photography, with its adaptation for fluorescence detection, is a modification of the general technique of anterior chamber slit lamp fluorophotometry. Scheimpflug photograph is an imaging technique that is relatively new and is used for assessing lens abnormalities such as cataract. This is an accurate, reproducible and observer-independent system that can be used to classify cataract. Scheimpflug photography has been in use over the past decade as a non-invasive tool for examination of the lens. It captures several types of images, including single photographic slit sections of the anterior segment and retroillumination images of the lens, and can be used as a postoperative imaging tool to calculate the position of an intraocular lens implant. A unique feature of this imaging technique is the ability to create a three-dimensional reconstruction of a lens by capturing several static slit images, providing sufficient information to determine the volume of opacity of the lens and the exact location of the opacity (Sachdev et al.,2002).

In Scheimpflug photography the optical axis of the excitation light and axis of the film / detector equipment are parallel to each other. A long depth of field objective located at one angle with respect to the axis of the excitation light is used to image scatter or fluorescence from the lens onto the film (Mayor et al.,1985).

The Topcon SL 45 camera, modified for Scheimpflug photographs is the best instrument available for fluorescence imaging. Scheimpflug photography is becoming a standard method to monitor modification of lens fluorescence in relation to age and cataract formation . This is normally correlated with visible Scheimpflug densitometry to monitor lens opacification and scattering (Lerman et al.,1981).

Instrumentation:

The Fluorotron Master has become through the years the standard instrument for vitreous fluorophotometry and also for anterior segment fluorophotometry after being adapted. The instrument consists of an optoelectronic unit and a computerized system of data acquisition and processing. This unit is basically a fluorophotometer in which a beam of exciting blue light is delivered by a pair of lenses that also pick up .the fluorescent light and direct it into a halogen tungsten incandescent bulb and the exciter and barrier filters each consisting of double interference filters that result in negligible spectrum over lap (Mayer et al.,1985).

The photomultiplier is operated in a single photon counting mode. Each photon is converted into an electric pulse and the electric circuit counts the number of pulses in a given interval. The major advantage of this mode is noise reduction by ignoring pulses of low amplitude, which are mostly generated by noise processes. The noise reduction increases the sensitivity of the instrument (Mayer et al.,1985).

The optical system is coupled to the optics of the eye and no contact lens is necessary to image objects as posteriorly as the retina. The excitation beam is delivered through one part of the lenses and the fluorescence is gathered through another part. The intersection of these two paths creates at the focal plane a volume of measurement. The motion of the second lens causes this volume to be translated along the axis thus sampling at different positions in the eye .A reading is obtained for each discrete step starting at a

position appearing to be posterior to the retina and ending at a position anterior to cornea. Each measurement is calibrated by an automatic reading of an internal fluorescent glass. The eye of the subject is aligned by moving a chin rest until the target is centered in the pupil and the iris is brought into focus. The appropriate focus is determined by a split-image range finder. The patient fixates on a target to insure stability of the eye and relaxation of accommodation. The target remains visible during the scan but the operator's viewing port is closed .The optoelectronic system is controlled by a computer which directs the operator throughout the procedure by prompting the choice of items from different menus. The operator initiates the scan which is automatically performed and displayed on a screen in concentration units distance from the retina. The scan is then stored along with the patient data on magnetic diskettes. The results can be printed out in graphic and digital forms on hard copy. The flexibility of the computer can be used to process the data by using appropriate programs (Lerman et al.,1981).

Spread Function And Axial Resolution:

These concepts were introduced to quantitate the effect of a large fluorescence peak in the reading in its vicinity. More specifically, in a compartment when the fluorescein concentration is high or the lens which autofluoresces, an artifactual reading will be obtained even if fluorescein is absent from this compartment. This artifact is primarily due to the finite axial length of the probing volume that is scanned across the eye. This volume is determined by the optics of instruments and the eye. The artifact may also depend on factors such as the scatter in the lens and choroid .It was demonstrated that this artifact is related to the fluorescence peak generating it and can thus be defined as a function. This Function is referred to as the spread function of this peak (previously referred to as tailing).The distance at which this spread function reaches a given relative value is called the (axial resolution) previously referred to as depth resolution .The spread function of the lens is measured by performing scans prior to injection of fluorescein. The location of the posterior capsule of the lens was taken from the scan as the position where the fluorescence reached half the peak value.The rationale of this procedure is that when the probing volume is exactly located at the lens interface, only half of it is within the lens thus yielding a reading that is half the reading inside the lens (Zeimer et al.,1982).

Reproducibility:

Reproducibility is defined as the spread of repetitive readings. Ideally it can be assessed by performing many successive measurements. However because the level of fluorescence evolves with time, the difference between two consecutive measurements few minutes apart is assessed. This provides data from many eyes rather than many data points from individual eyes which is a more tasking procedure for the subjects (Mayer et al.,1985).

Fluorotron Master has several advantages over other commercially used instruments. The elimination of the need for a contact lens is a substantial improvement in comfort of the patient. It allows better performance of sequential measurements which is tasking on the subject with the use of other instruments. Good alignment is important; otherwise light can be obstructed by the iris and off axis scanning will produce optical degradation. The "Fluorotron Master" provides a reliable alignment and an ipsilateral fixation target for the subject .Fluorometric readings are influenced by the artifactual contribution due to the spread function of lens signals. These artifacts can be reduced by proper instrumentation; but further reduction of the artifacts were achieved by the use of correcting algorithms. The lens fluorescence spread function is accounted for by subtracting the pre-injection scan from the later scans (Mayer et al.,1985).

Evaluation Of Light Loss In The Lens:

Two methods have been proposed for evaluation of the lens transmittance (the ratio between the transmitted and incoming light intensities). In the first method, the subject matches metametric colors. By comparing the result with the expected rhodopsin spectrum, the filtering effect of the lens is deduced .This test is subjective and requires dark adaptation. The second method measures the ratio between the intensities of the anterior and posterior specular reflections of the lens (known as Purkinjie Samson images) (Coren et al.,1982).

The rational is based on the fact that the fluorescence of the lens is relatively constant along its anteroposterior axis. However when scanning the lens with a fluorophotometer, a decrease in the fluorophotometric reading is observed as the probing volume is focused more posteriorly(Jacobs et al., 1981).

Clinical Applications Of Ocular Fluorophotometry

I-Aqueous Fluorophotometry:

A) Fluorophotometry And Cataract Surgery:

The results of cataract surgery and visual recovery vary in the postoperative period, but in the long term they are highly successful. Failure in otherwise normal eyes is related to poor placement of the implant residual soft lens matter, posterior capsule thickening, uveitis from surgical trauma low grade infection or cystoid macular edema .Breakdown of the blood ocular barriers may occur in these conditions and has been implicated in the pathogenesis of many of these problem. Anterior segment fluorophotometry is an objective reproducible and simple technique for measuring the degree and duration of breakdown of the (BAB) and in following the sequential recovery of the BAB for the few postoperative months after cataract surgery whether associated with an implant or not or whether associated with other procedures like keratoplasty (Sanders et al., 1982).

The fluorophotometer measures anterior chamber (AC) fluorescence. The mean AC fluorescence is 301 ng/ml with a range of 140 ng/ml to 560ng/ml. Recovery of the BAB has been followed by iris angiography which gives a qualitative assessment but anterior segment fluorophotometry enables a quantitative measure of recovery of the BAB. The recovery of the blood aqueous barrier was found to be unaffected by factors such as a limbal or cornea section, position of the implant or the use of preoperative topical indomethacin (Ferguson et al.,1991).

B) Posterior Chamber Lens Implantation And Anterior Segment Barrier Function Evaluation:

Posterior chamber I.O.L implantation after extracapsular cataract extraction is the method of choice for implant surgery because this method affects the anterior segment less than any other methods of lens implantation. The postoperative effects on the anterior segment of P.C implanted eyes versus E.C.C.E only were evaluated by fluorophotometric technique (Kraff et al., 1980).

Fluorophotometry reveales that the dye (fluorescein) leakage into the aqueous is different depending on lens location, i.e. whether in the bag or

out of it. In bag fixation showed less leakage . Furthermore, lens material is not always free from the ethylene oxide gas that is used for lens sterilization. Residual ethylene oxide gas has a close relationship with postoperative intraocular inflammation (Schiffarth et al., 1984).

C) Fiuorophotometric Evaluation Of The Functional Parameters Of The Cornea:

Fluorophotometric evaluation of corneal endothelial permeability in "PERK" study patients:

Anterior radial keratotomy a surgical procedure for the correction of myopia was previously evaluated by the "PERK" (prospective evaluation of radial keratotomy). The operation as originally performed by "SATO" consisted of anterior and posterior radial corneal incisions (Yamaguchi et al., 1982).

A comparison of endothelial permeability between operated and non operated eyes using fluorophotometry was done on 24 hours and 6 months after surgery. Aqueous humour flow rates and anterior chamber elimination coefficients were significantly higher 24 h after surgery. Six months later there was no more significant difference in corneal permeability between operated and unoperated eyes (Hull et al., 1983).

D) Fluorophotometric Evaluation Of Endothelial Permeability Of The Cornea In Extended Contact Lens Wearers:

Anterior segment fluorophotometry was done to evaluate the endothelial permeability of a group of extended contact lens wearers versus another group of the same age and noncontact lens wearers. No difference in endothelial permeability or rate of aqueous flow was found between the two groups in more than 18% of patients (Carbon et al.,1988).

E) Iris Angiography:

Iris angiography is a useful means for the evaluation of anterior segment circulation in darkly pigmented iris like Oriental brown iris. And there was the remarkable change in iris microvascular circulation only after tenotomy of multiple muscles including vertical rectus muscles(Kwon et al., 1998).

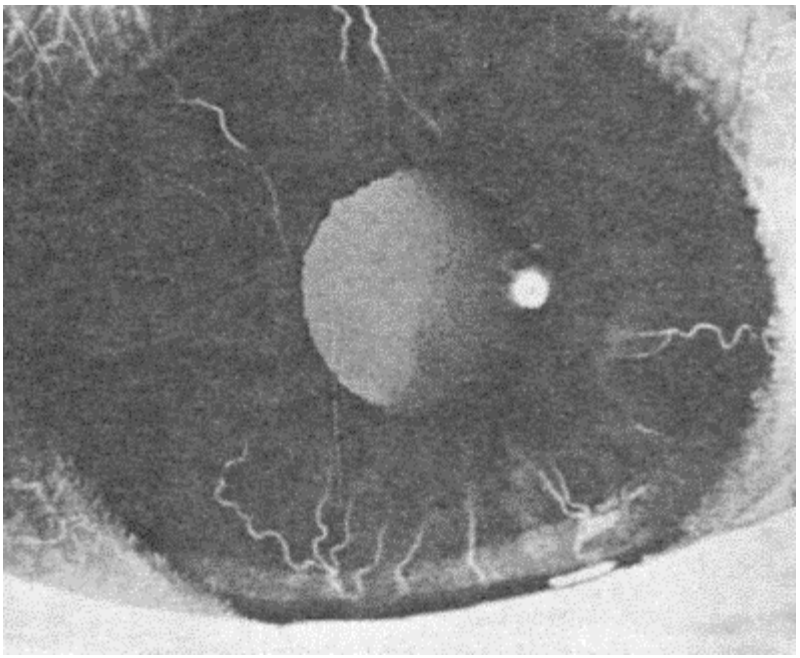

(figure 14) Iris angiography quoted from
Kwon SI, Shin MC, Choi DG. The Evaluation of Anterior Segment Circulation after Strabismus Surgery by using Indocyanine Green(ICG) Iris Angiography. J Korean Ophthalmol Soc. 1998 Dec;39(12):3069-3077. Korean.

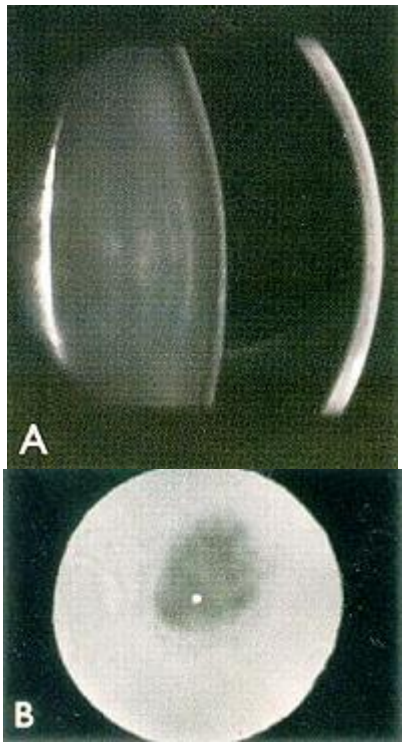

(figure 15) Scheimpflug slit photograph (A) and retroillumination image (B) illustrating a dense posterior subcapsular opacity
Ueda Y, Duncan MK, David LL. Lens proteomics: the accumulation of crystallin modifications in the mouse lens with age. Invest Ophth Vis Sci 2002; 43(1): 205-215

Ultrasound Biomicroscopic Anatomy Of The Normal Eye And Adnexa

The Cornea:

The superficial location of the cornea permits the use of higher frequency transducers (75MHZ or more). This allows a better definition of small distances such as epithelial thickness (Pavlin et al.,1991).

The corneal layers can be well differentiated by UBM. The reflection from the surface of the epithelium forms a smooth line in normal eyes that can be differentiated from Bowman's membrane, which forms a distinct, highly reflective line just below the reflection from the epithelial surface. The corneal stroma reveals a low, regular internal reflectivity. The endothelium cannot be differentiated from Descemet's membrane, but together they form a single highly reflective line at the posterior corneal margin (Pavlin et al., 1993).

The corneoscleral junction can be differentiated because of the lower internal reflectivity of the cornea compared to the sclera. This difference is most likely due to the difference in histological structure of these two regions. The smooth lamellae of the corneal stroma are less reflective than the irregular collagen bundles making up the sclera (Anderson et al., 1991).

The zone of change in reflectivity is not a clean line, but shows a gradual transition from the cornea to the sclera. The inner junction is generally referred to as Schwalbe's line. This junction is often not clearly defined on UBM. Occasionally the inner line is hypertrophied and can be imaged as a highly reflective internal band (Pavlin et al.,1991).

The surgical limbus as seen on examination of the external aspect of a normal eye is located approximately 1mm anterior to the scleral spur. This represents the transition between conjunctival tissues and corneal epithelium (Kavickhoff et al.,1992).

Measurement of corneal thickness can be done by various methods. Great care must be taken to produce a section perpendicular to the corneal surfaces. This is done by maximizing the brightness of the signals from the

epithelial and endothelial surfaces in a way similar to biometry techniques with conventional ultrasound (Reinstein et al.,1993).

The Sclera:

The normal sclera has a relatively high reflectivity compared to the cornea. This high reflectivity allows definition of the corneoscleral junction, and usually allows scleral tissue to be differentiated from the less reflective episcleral tissue, and the less reflective ciliary body and peripheral choroids (Avitabile et al.,1998).

It is essential to be as perpendicular as possible to the scleral surface for accurate measurement. The sclera is generally thickest in the region of the scleral spur. The scleral spur forms an important land mark for orientation and measuring distances in the region of the angle of the anterior chamber (Pavlin et al.,1993).

The Anterior Chamber:

The central anterior chamber can be imaged from the internal cornea to the lens surface. Careful technique is required if measurement of axial anterior chamber depth is desired. This can be accomplished at the time of examination by careful attention to perpendicularity of the sound beam to the cornea and the lens interfaces (Pavlin et al.,1992).

Measuring the axial distance from the internal corneal surface to the lens surface is facilitated by the ease of distinguishing the iris from the lens surface. This can be difficult with eyes with very small pupils using conventional ultrasound. Anterior chamber depth can be measured at a point other than the axial position. The distance from the cornea to either the iris or lens can be determined at any of these points. In a series of normal eyes the average axial anterior chamber depth measurement was found to be 3128±327μ (Woo et al.,1999).

The Anterior Chamber Angle:

The corneoscleral junction and scleral spur can be distinguished consistently with UBM. The scleral spur is a very useful landmark presenting a constant reference point for measurement in the angle region.

Measurement of the degree of anterior chamber angle opening based on UBM consists of taking a point on the internal ocular wall 500μ anterior to the scleral spur (which would fall on the trabecular meshwork) and extending a line from this point perpendicular to the plane of the trabecular meshwork to the opposing iris. The length of this line can be then measured, this measurement can be called angle opening distance (AOD) (Pavlin et al., 1995).

Results of measurement in normal cases were found to be 347±181μ for AOD at 500μ from the scleral spur. Angular measurement in degrees is easily made but difficult to define because of the anatomic variations in angle configuration. It is essential to designate the position of the apex, and to designate the points at which the arms of the angle touch the iris and the inner corneoscleral wall. The angle formed with the apex at the iris recess and the arms passing through the point on the meshwork 500μ from the scleral spur and the point on the iris perpendicularly opposite, is termed the trabecular-iris angle (θ1). This angle averaged 30±11 degrees in a series of normal eyes (Milner et al., 1994).

Measurement of angle opening can vary with changes in the state of iris dilatation. Subtle variations in iris curvature around the periphery will include small differences in measurement. This requires documentation of the precise radial position in which the measurement was made (usually designated in clock hours), and control of variables such as papillary dilatation (Pavlin et al., 1993).

The Iris:

The iris is well imaged in cross section by UBM. The iris recess varies in depth in normal eyes and can be outlined by UBM. The iris and ciliary body converge in this region and insert into the scleral spur. The area under the peripheral iris and above the ciliary processes is known as the ciliary sulcus. This is an important anatomical space, especially with regards to intraocular lens implantation. The iris shows subtle variations in surface curvature. The stroma shows a relatively low reflectivity. Occasional small spaces are seen in the iris stroma (Carassa et al., 1998).

The epithelium forms a constant, relatively thick, highly reflective layer on the posterior iris surface. This highly reflective line defines the posterior iris border and can be quite useful when one is differentiating intra-iris

lesions from lesions behind the iris. The epithelium can also be followed around the iris margin in cases of ectropion uvea (Caronia et al., 1996).

The overall iris curvature can be clearly outlined by UBM. A straight iris profile is usually found in normal patients. This contrasts with the anterior bowing seen in papillary block (Anderson et al., 1991), and the posterior bowing seen in some patients with pigmentary glaucoma (Kavickhoff et al., 1992).

Measurement of iris thickness requires precise definition of iris position. The iris normally shows variations in thickness in different regions. Histological studies show that it is generally thinnest at the iris root and thickest near the pupillary margin. In addition there are variations in the thickness depending on the presence of crypts, and the state of dilatation and constriction. The pupil size is constantly variable within a small range in the absence of pharmacological agents (Potash et al., 1994).

The position of iris measurement can be defined with reference to the scleral spur. Three points can be used to measure the iris. A line from the point on the trabecular meshwork, 500μ from the scleral spur, run perpendicularly through the iris and extended to the ciliary process. This distance is termed the trabecular-ciliary process distance (TCPD). Iris thickness along this thickness was termed ID1 (average thickness = 372±58μ). The iris ciliary process distance that defines the ciliary sulcus depth can also be measured along this line. Other possible points of iris measurement include, a measurement 2mm from iris root (ID2; average thickness =457±80μ), and at its thickest point near the pupil (ID3; average thickness =645±103μ) (Pavlin et al., 1992).

Other measurements that can be made include the zone of iris-lens contact distance (ILCD) (average distance in normal eyes is =1388±370μ) and the angle at which the iris leaves the lens (θ2; average =12±3°). Another interesting measurement is the angle the makes to a tangent on the scleral surface (θ3). This measurement can be significant with regards to blind surgery below the iris, such as transscleral intraocular lens fixation. This angle measurs an average of 30±7° in one series of normal eyes. The angle of the ciliary processes make to the scleral surface can also be measured (θ4; average =52±18°) (Brown 1992).

The Ciliary Body And Ciliary Processes:

The entire ciliary body can be clearly defined by UBM from the ciliary processes to the pars plana. The ciliary processes can be quite variable in configuration (Pavlin et al.,1995).

By UBM it is possible to visualize the ciliary zone and to make a diagnosis of laxation or sublaxation of the lens and so to choose the best surgical approach for its extraction. After IOL implantation, anterior segment may be obscured by corneal edema. With UBM examination the incarceration of the IOL in the pupil was detected. In other cases with anterior chamber IOL, UBM examination revealed the entrapment of the IOL loop in the corneoscleral wound (Avitabile et al., 1997).

The appearance will vary depending on whether the section is passing through the processes or the valleys between the processes. Not infrequently fine lines can be seen on the under surface of the ciliary body, most likely indicating zonular fibers in this region. The anterior vitreous face is occasionally visible (Watson et al.,1985).

The Lens And Its Zonules :

The anterior zonular surface can consistently be imaged by UBM. The appearance of the zonules is that of a medium reflective line extending from the ciliary process to the lens equator. This may indicate the degree of zonular tension. Optimal visualization of the anterior zonule requires that the focal point of the transducer be in the zonular region (Pavlin et al., 1995).

Basic Considerations In Ocular Ultrasonography

Tissues possess three important acoustic properties. These properties are attenuation, reflectivity and speed of sound that can be further subdivided into specular and scatter ultrasound imaging (Foster et al., 1984).

Principles Of Pulse Echo [Backscatter] Imaging:

Ocular imaging with ultrasound involves the generation of an ultrasound pulse from the transducer in response to a brief electrical stimulation. The pulse propagates through a coupling medium (such as water or artificial tears) and encounters the tissues of the eye. At each interface, ultrasound is partially reflected back toward the transducer. Some of these reflected echoes are reconverted into a radiofrequency electrical signal. These signals determine the distances to the various interfaces. This is referred to as an amplitude scan or A scan. It represents the reflectivity along one line and forms a single line on the monitor. A two dimensional image, or B scan is then formed by rotating the transducer about a fixed axis so that the final video image presents a two dimensional cross section through the eye (Anderson et al., 1991)

Tissue Reflectivity:

Reflectivity is perhaps the most important acoustical property of the tissue imaging components. At the larger tissue interfaces specular reflection take place. The strength of these signals depends on the acoustic properties of the tissues forming the interface, and the angle of the interface with respect to the transducer. At small tissue structures, ultrasound is scattered over wide range of angles. Of the reflected ultrasound, only a small fraction will be detected and converted into image information (Foster et al., 1984).

Speed Of Sound:

In ultrasound imaging, the speed of sound allows us to convert time of light into distance. The speed of sound is inversely proportional to the compressibility and density of a material. The highest speed of sound in the eye is observed in scleral tissue (1622m /s), whereas comparatively lower speed of sound is observed in the ciliary muscle (1554m/s) and iris (1542m/s) (Foster et al., 1984).

Specular Reflection And Transmission:

Ultrasound waves obey many of the laws of geometrical optics. For example; Snell's law which states that the angle of incidence equals the angle of reflection. The acoustic impedance describes the elastic properties of the tissues. The relative acoustical impedance for the cornea = 1.55, sclera =1.61, lens =1.73, vitreous =1.54, and retina = 1.55 (Thijssen et al., 1983).

Scattering From Tissue:

Scattering of ultrasound from a target tissue constitutes the critical information in the ultrasound image of the soft tissue. Some of these randomly scattered waves (the back scatter portion) arrive back at the transducer where they are summated. The brightness of a given tissue on the scanner monitor is directly proportional to the degree of backscatter. The sclera has backscatter 2-5 times higher than other ocular tissues (Pavlin et al., 1995).

Resolution And Penetration:

There is a constant need to make a compromise between resolution and penetration, in order to obtain an image of maximum resolution. The best focus is achieved at the focal length (R) of the transducer and the width of the beam expands as we move away from the focal plane. The region over which the beam remains reasonably well focused is called the depth of field (DOF). The focusing characteristic of the imaging transducer is usually chosen such that the tissue of interest lies within the depth of field. (Kavickhoff et al., 1992).

Basic Physics Of High Frequency Ultrasound Imaging:

Ultrasound Biomicroscopy (UBM) is high resolution acoustic imaging of ocular structures. In order to be useful clinically in intact eye, a backscatter technique (pulse-echo) similar to that used in conventional B-mode scanners must be employed (Sherar et al., 1988).

B-scan Mode:

It is used predominantly for architectural information (cross sectional images of the globe and orbit) (Yanoff et al., 1999).

It is useful as an imaging method measurement tool, and a mean of characterizing ocular tissues, but resolution has been remained limited because of the ultrasound frequency used. As a general rule, higher frequency ultrasound results in greater resolution and more accurate measurement, but at the expense of decreased tissues penetration (Pavlin et al., 1991).

Transducer probes of conventional ultrasonography are enclosed in a hand held container. A small motor within the hand piece moves the ultrasonic probe in a rapid sector scan to create cross sectional B-scan image (Yanoff et al., 1999).

The development of transducers for very high- frequency ultrasound imaging was based on the polymer Polyvinylidene Difluoride (PVDF). These transducers were sensitive over a very broad range of frequencies. (Brown et al., 1992).

By 1984, 13 MHZ polymer devices were being used to map the acoustical properties of human tissues. This system demonstrated microscopic (15 micron) subsurface resolution in living tissue. The success of this technique rapidly lead to development of the first B-scan imaging system.

This system was adapted for ocular imaging by Pavlin et al., 1995 resulting in UBM. UBM is distinguished from conventional ultrasound B-scan imaging approach, which is basically a transmission imaging method. The reduced penetration of high frequency ultrasound rendered the eye an ideal clinical application for UBM.

B-scan ultrasonography is an important adjuvant for the clinical assessment of a variety of ocular and orbital diseases. With understanding of the indications for ultrasound and proper examination technique, one can gather a vast amount of information not possible with clinical examination alone (Thomas and Rhonda, 2005).

B-scan ultrasound is most useful when direct visualization of intraocular structures is difficult or impossible. Situations that prevent normal examination include lid problems (e.g. severe edema, partial or total tarsorrhaphy, keratoprosthesis, corneal opacities (e.g. scars, severe edema),

hyphema, hypopyon, miosis, pupillary membranes, dense cataracts) (Thomas and Rhonda ,2005).

Sound occupies the range from 10 MHZ to 20 MHZ of the acoustic spectrum. The ultrasonic frequency occupies from 20 MHZ to 100 MHZ. Ultrasound has numerous applications, perhaps the most important of these is Sonar. In body imaging, where significant penetration of the tissues is needed, frequencies between 3.5 MHZ to 5 MHZ are incorporated (Pavlin et al., 1995).

These frequencies have the ability to penetrate the tissues to a depth 15 cm to 20 cm and still return signals of sufficient strength to form an image. As the frequency increases, the ultrasound is more strongly attenuated, reducing penetration. Higher frequencies (7 MHZ to 10MHZ) can be used in imaging small parts such as visualization of the eye, where penetration of 4 cm to 5 cm is sufficient (Pavlin et al., 1995).

Three-Dimensional Imaging:

This is a method for three-dimensional reconstruction of UBM images. It is performed through a unit that incorporates a 50 MHz transducer, giving a resolution of approximately 50 microns, a field of view of 5mm and a scan penetration of 4 to 5 mm. All scanning is performed with the patient supine under standardized room lighting conditions. Eyecup immersion scanning is performed with a real-time image under rate of eight frames per second. Multiple, sequential, parallel, aligned images are acquired using a probe along the z-axis at a precise constant velocity to complement the x- and y-axis sweep of the transducer. The controlled scanner movement along the z-axis produces a real-time ultrasound panoscopic view of the eye with a slice thickness of 50 microns. These slices are obtained by digitizing the real-time videotape output of the UBM with a digital video frame-grabber, using 640 by 480 pixels at eight frames per second. Thus, three-dimensional reconstruction of a cyst located at the iridociliary junction indenting the peripheral iris and narrowing the anterior chamber angle. The multiloculated nature of the cyst cannot be appreciated in a two dimensional image (Ritch et al.,1997).

Instrument And Method Of Examination

The high- frequency, high resolution UBM has a (50 MHZ) transducer and achieves a resolution of approximately 50µm. The field of view is 5 mm, with a scan penetration of 4 to 5 mm. All scanning was performed under standardized room lighting conditions. The operator is usually seated behind the patient's forehead for stability. The small indentation in the scanning head allows one to hold the probe more securely. The probe is held close to the transducer end to improve fine control (Lezzi et al., 1996).

Eye cup immersion scanning is performed with the patient in the supine position under topical anesthesia, a 20mm eyecup is inserted between the eyelids and filled with 2.5% methylcellulose or saline solution, the transducer is placed into the coupling medium 2mm to 3mm from the ocular surface and held perpendicular to the surface being scanned, scans are recorded onto super- VHS videotape with real-time video output. Some forms of fixation devices that the patient can look at with the eye not being examined is helpful because this produces stability in the eye being examined. (Pavlin and Foster, 1995).

Modes of examination:

Ultrasound traverses in air very poorly, so that a coupling medium is required. Scanning using saline solution provides a resolution similar to or better than resolution of images obtained by methyl cellulose. But 2.5% methyl cellulose is used more because it has low sound attenuation, safe, and has a certain degree of viscosity to prevent rapid fluid loss. It is necessary to remove air bubbles caught in the concave surface of the transducer by immersing the tip in water and massaging the tip very gently with a bent swab (Pavlin et al., 1995).

Examination of the eye is either by using eye cups or water bath:

1- Eye cups:

Eye cups for UBM are similar to eye cups have a smooth flanged inferior margin that fits between the lids and holds them open (Pavlin et al., 1995).

A new cup is molded from polysiloxane material with an inner polycarbonate supporting ring. By this way it can fit well to the eye so the saline can be substituted by methyl cellulose (Kapetansky, 1997).

The superior lid of the cup is placed under the upper lid with the patient looking down. Then the lower lid is drawn down and placed over the inferior lip. When the lid speculum is in position it has the shape of a bowl which must be filled with viscous fluid e.g. Methyl cellulose. The oscillatory tip of the scanner probe must be submerged in this fluid within 1mm to 2mm from the eye surface to obtain oscillatory images (Pavlin et al.,1995).

2- Water bath and coupling media for ultrasound biomicroscopy:

This technique consist of instilling local anesthetic, applying colloid on to the skin, sticking the opening of the eye drap to the ring which is designed to hold the edges of the drap. Wire speculum can be used to hold the eye open. Water bath disadvantage is that it requires a long time to setup its component (Feijoo et al., 1997).

Ultrasound biomicroscopy scanning can recently be done in the sitting and probe position and to develop a reliable method for performing UBM in those positions the prone which is suspended from the articulated arm is removed and reattached to the arm up side-down for use in the prone position and horizontally for use in the sitting position. A latex tono-pen tip cover is attached to the edge of the eye cup and is placed over the transducer through the small hole over the tip of the tono-pen cover. This method can expand the ability of the UBM to examine alterations in anatomic relationships among anterior segment structures between the supine, sitting and prone positions (Esaki et al., 2000)

Corneal Diseases

Corneal diseases can generally be assessed well by direct slit lamp biomicroscopy. Most pathological changes occurring in relatively clear corneas can be observed directly, and the depth of corneal changes determined. However, slit lamp examination becomes difficult when the corneal lesion is extensive, or when the cornea is covered e.g. by a conjunctival flap. Under these circumstances, UBM allows assessment of internal corneal changes, of corneal dimensions, and of underlying changes of the anterior chamber (Byrne et al., 1992).

Accurate determination of the measuring points as well as precise measurement of the corneal thickness is essential for corneal thickness mapping. The pachymeters allow accurate measurement of the corneal thickness in the transparent central cornea, but do not provide accurate location data so that mapping with these techniques is unsatisfactory. Using UBM, measurement of corneal thickness can be done without touching the cornea, and locations can be determined even in a clouded cornea (Wada 1997).

Although a change in the corneal thickness during a single day was reported, no clinical differences were found with the various measurement times. No significant differences in corneal thickness was found between the left and right eyes, regardless of sex. Changes in refractive index caused by the coupling fluid result in only a negligible error in thickness measurement in vivo (Pavlin et al., 1995).

Variations in corneal thickness from small deviations of fixation were minimized by requesting the subject to focus on a point on the ceiling during scanning, errors from slightly eccentric fixation produce only negligible errors in corneal thickness measurements. Corneal thickness mapping can contribute to the evaluation of the cornea following refractive surgery or in pathologic conditions to evaluate postoperative healing (Wada 1997).

Corneal Edema And Leucomas:

UBM is used to investigate corneal edemas and leucomas and their progression. It is useful in finding the right surgical approach in this type of eye pathology.(Avitabile et al., 1998).

Edemas can affect the epithelium or the stroma or both. Epithelial edema is easily visible by slit lamp; by UBM, the first layer (epithelium, Bowman's membrane and interposed space) appears thicker and more reflective, due to the hydropic intra- and extracellular swelling or to small intercellular vesicles, which increase the interfaces at the ultrasound flow. Corneal edema can occur from many causes, most involving some form of endothelial pathology. There is an increase in the thickness and reflectiveness of the normal stromal layer, stromal edema can be localized or diffuse; for the structural change in the corneal lamellae, which is due to the appearance of large interlamellar vesicles (Pavlin et al., 1991).

In bullous keratopathy, bullae can be imaged as a separation of the epithelium from Bowman's membrane. The thickness of the corneal stroma can be measured independently of the epithelial thickness by measuring the distance from the Bowman's membrane reflection to the endothelial surface. This may prove valuable in the assessment of graft rejection or other causes of corneal thickening (Avitable et al., 1998).

UBM examination was performed for patients who had suffered a perforating corneal wound, in some cases it could visualize the scar which crossed the cornea in its whole thickness appearing as a hyperreflective area. In other cases of post-traumatic chronic corneal edema, two intrastromal foreign bodies could be located, which were not seen by slit lamp or radiographic examination as they were radio-transparent. These were visualized like a small area with a very high reflectiveness into the stroma which was thicker and more reflective (Milner et al., 1994).

In other cases after caustic trauma with chemical injury the corneal scars were so large and serious that corneal transplantation was necessary, UBM gave very useful information about the condition and the structure of the anterior segment which allow to plan the surgery. Also the anterior segment structures can also be evaluated behind a completely hyperreflective some what calcified irregular thick cornea. This is an essential evaluation before doing penetration keratoplasty or keratoprothesis (Morinelli et al.,1996).

In other patients keratoprosthesis was performed because of the severe corneal damage. UBM in these cases is helpful before surgery, in which the cornea appeared hyperreflective, irregularly thickened and some what calcified; the anterior surface of the iris and the lens were covered with fibrous membranes, some synechiae were present between the cornea and

the iris and the lens. It is possible to study the keratoprosthesis which appears like an anatomic section (Falcinelli et al., 1997).

Keratoconus:

UBM was performed to study the mild, moderate and severe forms of Keratoconus and to determined corneal thickness and the keratoconus index (KI)(which is the ratio between the peripheral corneal thickness and the thinnest central thickness) and to compare these data with the severity of the disease determined using videokeratography and ultrasound pachymetry. Using UBM it is possible to dynamically display the patient's cornea, to study the area of conus together with the thinnest site and to freeze and store the appropriate image for subsequent measurements (Wheeler et al., 1992).

It allows the accurate measurement of the corneal thickness directly in the thinnest part of the cone, and it might explain the results of the measurements of the corneal thickness which are different from those obtained using ultrasound pachymetry. The peripheral determination of the corneal thickness was performed at a site placed 2.5mm from the central measurement (Bron 1988).

This observation is in agreement with the statement of Holland et al that suggested a normal thickness of the cornea outside the conus. In addition (KI)was calculated using UBM in order to follow the disease. Besides the existing classifications based on the modification of the corneal curvature, it may also be possible to attempt a new classification according to the progressive corneal thinning calculated by means of UBM (Amsler 1946).

In a study made by Avitabile et al 1998 the mean corneal thickness at the thinnest part of the conus was 0.396mm (range: 0.310-0.457mm), while the mean peripheral measurement was 0.568mm (range: 0.538-0.655mm).

Corneal Grafts:

UBM provides a new method of assessing corneal grafts. Aberrations at the graft-host junction can be assessed. This area is often difficult to visualize at the slit lamp because of the scarring present due to healing at the suture line and the frequent opacity of the residual host cornea. The problem is further complicated if there is any opacity in the graft itself (Pavlin et al., 1995).

Corneal Dystrophies:

UBM can image changes that occur in the weakly reflective regular corneal lamellae. The granules of hyaline material are clearly imaged on UBM. The granules which increased reflectivity and are located mostly in the superficial stroma (Pavlin et al., 1995).

Congenital Corneal Opacification By UBM:

The differential diagnosis of congenital corneal opacities was reached in a study performed by Nischal et al in 2002 on 13 children. They correlated their UBM finding with clinical and histological finding to confirm the diagnosis. They were able to discern Peters' anomaly in nine cases, (posterior polymorphous dystrophy and congenital hereditary endothelial dystrophy) in two cases and sclerocornea in two cases.

Peters' anomaly the normally hyperreflectivity of the Descemet's membrane/ endothelium was not seen in association with a central posterior corneal defect. Absence of Descemet's membrane and endothelium was confirmed histologically (Haddad et al., 1997).

Also, an unusual hypoechogenic region was seen in the anterior stroma on UBM examination. Histology revealed an absence of Bowman's layer with edema in the region adjacent to where Bowman's layer should have been, together with absence of Descemet's membrane(Bessho et al., 1998).

Clinically the cases of sclerocornea showed extension of opaque scleral tissue and fine vascular conjunctival and episcleral tissue into the peripheral cornea obscuring the limbus.The severity of scleralization varies from mild to complete but is usually bilateral in 90% of cases (Kenyon 1975).

Histologically the corneal epithelium showes secondary changes with absences of Bowman's layer in the affected areas. There is interstitial vascularization without inflammation and the stromal collagen fibrils are comparable to scleral collagen in size and organization. There may be irregular absence of both endothelium and Descemet's membrane or an abnormally thinned Descemet's membrane composed of multilaminar basement membrane (Myles et al., 1992).

Awan 1977 reported on one case that demonstrated the presence of Axenfeld-Rieger anomaly with Peters ' anomaly on UBM. The scarcity of previous reports may be due to the fact that young infants are difficult to examine, and gonioscopy to detect the iridocorneal adhesions is particularly difficult in an eye with a corneal opacification.

UBM can also demonstrate the presence of aniridia with corneal opacity (Eiferman 1984).

Refractive Surgery

Refractive surgery has become increasingly common over the past two decades, a variety of surgical and laser techniques have been used (Trokel et al., 1983).

Paralleling the growth of refractive surgery has been increased interest in the assessment of corneal topography, conventional keratometry and refraction, whether manual or automated, fail to evaluate the overall shape of the cornea, this is a significant shortcoming in refractive surgery, where surface topography varies from region to region (Mcwhae et al.,1999)

Computer-assisted photokeratocopy has been a major step forward in this area. It provides a map of corneal topography that is reproducible, however, photokeratoscopy does not produce a true cross-section analysis of the cornea (Mcwhae et al., 1999).

LASIK and Eximer laser photokeratectomy (PTK) are used for correction of refractive errors and the latter as a therapeutic method in superficial corneal diseases (Pavlin et al., 1994).

The excimer laser is capable of removing a small, controlled amount of corneal tissue with minimal damage to surrounding tissue. Monitoring the result of excimer laser treatment, UBM on the site of laser photoablation reveals the changes in surface configuration that take place. The anterior corneal curvature shows flattening. The normal superficial, double-layered appearance of the highly reflective epithelial surface and Bowman's membrane is replaced by a less clear division between the surface epithelium and the underlying stroma. This is probably due to loss of Bowman's membrane, with the resulting stromal-epithelial interface having a lower specular reflectivity (Falcinelli et al., 1997).

The double echo of the untreated region gives way to the single echo of the treated region where Bowman's membrane is absent, the stromal surface cannot be differentiated in the treatment region haze. UBM appearance of the junction area again showed the transition from the double line of untreated cornea to the single line of the treated cornea.(Falcinelli et al., 1997).

The cornea is distinctly thinner in the treated region and the superficial stroma showes irregular regions of increased reflectivity, which corresponded to the superficial corneal scarring. The regions of increased reflectivity from scarring outlines the superficial stroma, allowing differentiation between the epithelial surface and the stroma (Pavlin et al., 1994).

The major UBM features noted in corneas treated by excimer laser keratoablation are thinning of the treated zone and loss of the highly reflective echo that corresponds to Bowman's membrane. It has been shown histologically in vivo that Bowman's membrane is removed in the treated zone, this corresponds to the findings of UBM.(Pavlin et al., 1994).

Determining corneal curvature changes is possible using UBM and would be aided by more precise localization of the treatment zone's center. The ability to image the entire treatment region simultaneously would be helpful, with treatment zones of 5 to 6 mm in diameter, an ultrasound field width slightly greater than 6 mm would be required to image both margins simultaneously (Trokel et al.,1983).

Scleral Diseases

The exact anatomic classification of the scleral inflammation is mandatory to determine the need for treatment and the appropriate therapy. UBM thus provides a new method of imaging anterior scleral tissues and its diseases. Conventional ultrasound has been useful in detecting changes in posterior scleritis, but has limited application in anterior scleral diseases (Tuft et al., 1991).

UBM examination of the sclera can be performed at any point where the moving transducer can be placed directly over the area being examined. Generally these sites are anterior to the equator (Pavlin et al., 1993).

The diverse types of scleral inflammation often can be distinguished by typical slit lamp signs. The additional use of topical vasoconstrictors may be helpful in differentiating scleritis from severe episcleritis. However, severe episcleritis may not be distinguished by slit lamp examination from benign non destructive scleritis and necrosis.(Heiligenhaus et al., 1998).

Localized Scleral Staphyloma

Localized scleral staphyloma are uncommon, but can create a problem in the differential diagnosis of other causes of a black dot on the surface of the globe such as conjunctival melanoma or an extrascleral extension of a peripheral tumor (Pavlin et al.,1992).

Episcleritis:

Episcleritis can often be difficult to differentiate from scleritis on clinical grounds alone. UBM reveals thickened episcleral tissue without apparent involvement of the sclera. A clear margin can be observed between the episcleral thickness and the scleral surface. The sclera appears to be of normal thickness and normal internal reflectivity in this region (Watson et al.,1985).

Diffuse Sclreitis:

UBM shows an episcleral thickening with diffuse scleritis. There is also focal areas with decreased reflectivity, most probably representing the perivascular or scleral infiltration and edema. The sclera itself will show a

mottled internal reflectivity with areas of lower reflectivity scattered throughout the involved region. The sclera outside the involved region will shows a normal appearance with a uniform highly reflective sclera (Roa et al., 1985).

Nodular Scleritis:

UBM appearance of an acute scleral inflammation, will present clinically as a localized elevation, with thickening of the episcleral layer. Involvement of the sclera is manifest as a localized nodule of lower reflectivity than the surrounding sclera. The scleral nodule is differentiated from the surrounding by a distinct border extending about 2/3 of the way through the scleral substance. Clinically after resolution of the acute phase there is no obvious scleral thinning on clinical examination. However, scleral thinning was clearly present on UBM (Pavlin et al.,1992).

Necrotizing Scleritis:

Necrotizing scleritis by definition is scleritis resulting in regions of scleral thinning. In cases in which the sclera is thinned, UBM allows an objective method of assessing the degree of thinning (Böker et al.,1999).

Scleral Surgery:

Pars Plana Sclerotomy:

Since the introduction of Pars plana vitrectomy, the Pars plana sclerotomy has been considered to be a potential site for complications such as peripheral tractional detachment, retinal tears, and traction at the ciliary body, causing hypotony and recurrent vitreous hemorrhages (Fong et al., 1991).

UBM identifies the entry sites which show a high degree of variations. Most commonly, delicate membrane like strands will be observed. Most likely these strands will represent the fibrovascular materials as a feature of normal wound healing (Böker et al.,1999).

Vitreous incarceration was seen on UBM as echogenic strands converging toward an ultrasonically lucent site in the sclera. Images with no observed strands adhering to the sclerotomy sites were classified as grade 0,

and the images with the widest and thickest converging strands were classified as grade 3. All other images were graded between 1 and 2 (Kwok et al., 2001).

In a UBM study by Bhende et al.,2000 the incidence of fibrovascular proliferation following sclerotomies in diabetic patients was found to be much higher than in non-diabetics despite the absence of postoperative complications. This was believed to be due to biochemical changes in the vitreous of diabetic patients rendering the collagen sticker and more mobile.

UBM In Anterior Segment Tumors

Iris Naevus:

Iris naevus is a pigmented, flat or slightly elevated lesions, which is usually less than 3 mm in diameter. It is usually located in the superficial layers of the iris and it may occasionally cause mild distortion of the pupil and ectorpion uvea (Kanski 1999).

UBM appearance consists of a small moderately thickened iris lesion not extending posterior to the iris root and with or without distinctive anterior convex bowing. There is a hypoechogenic layer on the surface of these lesions, possibly indicating that the superficial layer was involved with a tumor plaque (Pavlin et al.,1992).

UBM may show the stuck on appearance when there is a distinct border between the lesion and the iris tissue, or the UBM may show uniform thickening with an uncertain margin between tumor and iris tissue. Pedunculated masses or collar shape similar to that seen with choroidal tumors breaking through bruchs membrane may be also seen (Pavlin et al., 1995).

Iris Melanoma:

Iris melanoma is a rare tumor that accounts for about 8% of all uveal melanomas. It's a very slow-growing tumor usually of low malignancy because it is composed of spindle cells. It is pigmented or non-pigmented nodule, which is at least 3 mm in diameter and 1 mm in thickness with a smooth or irregular surface located in the inferior half of the iris. Tumor vascularity is easier to detected in non-pigmented tumor whereas in a highly pigmented tumor it is often masked. Associated features include pupillary distortion, ectropion uvea and occasionally localized lens opacities. Angle involvement if extensive, may give rise to secondary glaucoma (Kanski 1999).

On UBM the tumor gives rise to a lobulated internal structure with variable internal reflectivity and cystic spaces that may represent vascular channels. Iris melanomas exhibit a wide range in acoustic back-scatter properties, whereas characteristics such as vascularity and necrosis might

contribute to this back-scatter characteristics which could be largely due to melanocytes distribution (Ursea et al.,1998).

Irido-Ciliary Cysts:

Iridociliary cysts usually presents as small localized elevation of the iris. UBM can diagnose cysts in these region, and appear as thin walled cysts, with no internal reflectivity, and occasional multiloculations. Total lack of internal reflectivity indicates fluid filled cyst and this feature eliminates and possibility of confusion with solid tumors (Pavlin et al.,1992).

Iris cysts are typically imaged as round or elliptic lesions with thick walls and a sonolucent cavity. Occasionally, dense fluctuating particles are seen in the cystic cavity (Augsburger et al.,1996).

In congenital non-pigmented iris cysts, these cysts are particularly rare. They are seen as translucent cysts in the middle or periphery of the iris and tend to enlarge and their pathogenesis remains controversial, entrapment of surface epithelium inside the eye during lens vesicle separation may be the cause (Margio et al.,1998).

UBM images of these cysts were no different from images of other implantation cysts. Photocoagulation has been used to puncture and shrink epithelial cysts. Multiple treatments may be required and despite treatment, recurrences are common. Producing a hole in the wall of an epithelial cysts may externalize it, therapy converting it into sheet like epithelial in growth (Solomon et al.,1996).

UBM In Limbal Dermoids:

Limbal dermoids are solids congenital lesions that typically appears the inferotemporal limbus.

These lesions contain a superficial stratified squamous epithelium, and the underlying elements that includes a varity of mesodermal derivatives including elastic fibers, muscle, dense connective tissue, blood vessels, cartilage, fat and so forth, additionally, hair follicles and sebaceous glands may be found(Grant et al.,1999).

UBM was helpful in ruling out a dermolipoma with typical posterior extension and osteoma. Most importantly, it was valuable in delineating the depth and extent of the lesion. it may not be possible for current clinical UBM to distinguish all of the above entities given the gross textural similarities of these tissues, however, the extremes in this list would probably be easy to differentiate with this technology(Grant et al.,1999).

UBM in Cataract Surgery

UBM For The Assessment Of The Ease Of Haptic Removal:

UBM can be used to assess the ease of the haptic removal before penetrating keratoplasty combined with lens exchange by evaluating the anterior chamber intraocular lens (IOL) haptics in eyes with poor corneal clarity resulting from pseudophakic bullous keratopathy. UBM can identify the presence or absence of fibrotic encasement and the degree of difficulty in removing the anterior chamber IOL haptics (Rutnin et al., 1997).

UBM also allows assessment of the adjacent angle for synechiae, providing alternative method when gonioscopy is impossible because of corneal opacity and allowing the surgeon to predict preoperatively the degree of difficulty that will be encountered in explanting the IOL (Rutnin et al., 1997).

UBM For Evaluation Of Long Term Stability Of Trans-Sclerally Sutured Posterior Chamber IOL:

UBM is performed postoperatively to determine the exact haptic position in relation to the iris base, ciliary sulcus, pars plicata, and parsplana (Hudde et al., 1996).

Before the development of UBM cataract surgeons did not have a reliable technique to check weather the IOL haptics were really situated in the capsular bag. Out of the bag location of an IOL is reported to cause pigment dispersion from the posterior iris epithelium (Irene et al., 1999).

Using the UBM for comparing the lens haptic position after phacoemusification with continuous curvilinear capsulorhexis (CCC)and extracapsular cataract extraction with linear capsulotomy, it was found that phacoemulsification using CCC is a safer method than ECCE using linear capsulotomy for IOL implantation in the capsular bag as CCC creates a true bag which facilitates predictable implantation of IOL and ensure that the IOL remain in the capsule (Irene et al., 1999).

UBM In Late Onset Recurrent Hyphema After Cataract Surgery:

Late onset recurrent hyphema is an uncommon complication of posterior chamber IOL implantation. Pathologic studies and indirect clinical evidence including iris transillumination defects and iris tucking have implicated haptic iris contact. Using UBM IOL haptics can be visualized and their relationship to surrounding structures can be assessed. Blood can be traced beneath the peripheral iris. This indicates that haptic iris contact is the source of bleeding and capsular fixation should make this complication less likely (Pavlin et al., 1994).

Figures of UBM are quoted from Atlas of Dr. Charles Pavlin1999, 2000 from internet (www.eyeubm.com/pavlin.atlas)

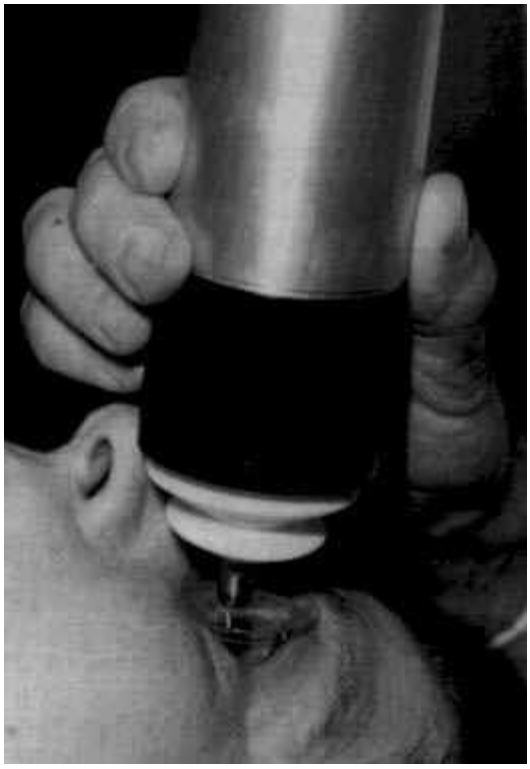

(figure 16) Method of examination of UBM
Atlas Pavlin 1999-2000.

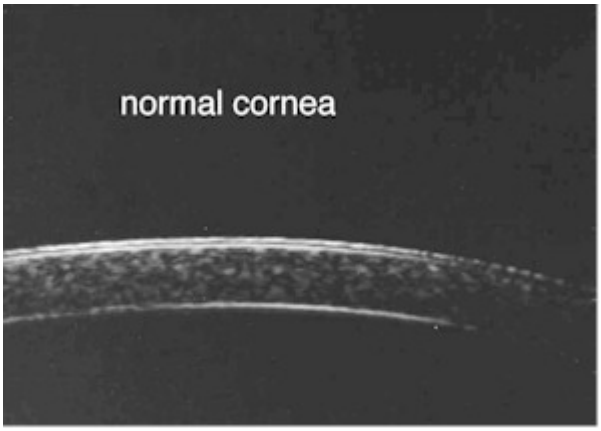

(figure 17) example of uses of UBM showing normal Cornea
Atlas Pavlin 1999-2000.

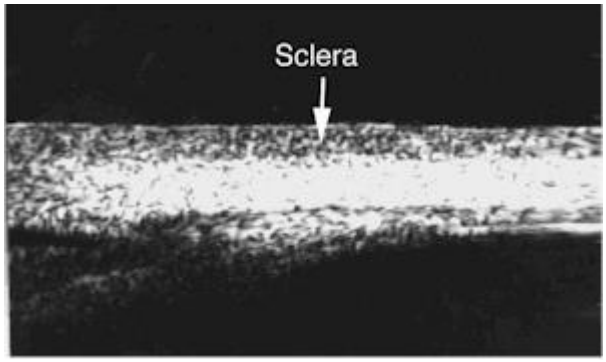

(figure 18) example of uses of UBM showing normal sclera
Atlas Pavlin 1999-2000.

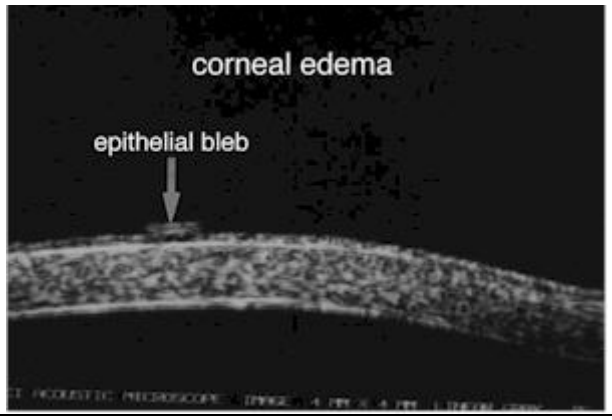

(figure 19) An example of uses of UBM showing Corneal Oedema arrow showing epithelial bleb
Atlas Pavlin 1999-2000.

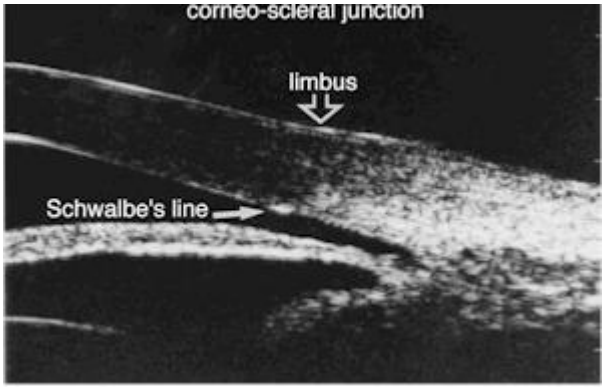

(figure 20) An example of uses of UBM showing normal corneo-scleral junction.
Arrow showing the limbus and the other showing Schwalbr's line
Atlas Pavlin 1999-2000.

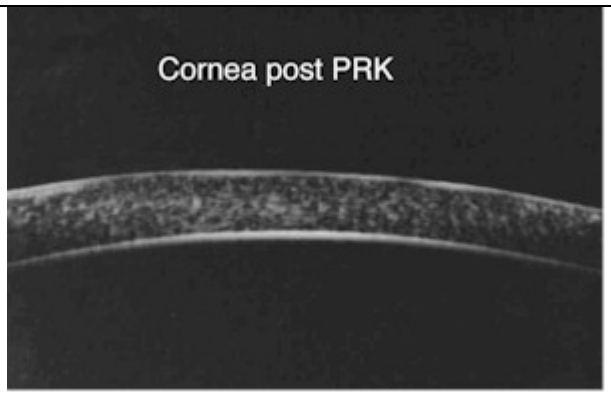

(figure 21) An example of uses of UBM showing shape of the cornea post PRK
Atlas Pavlin 1999-2000.

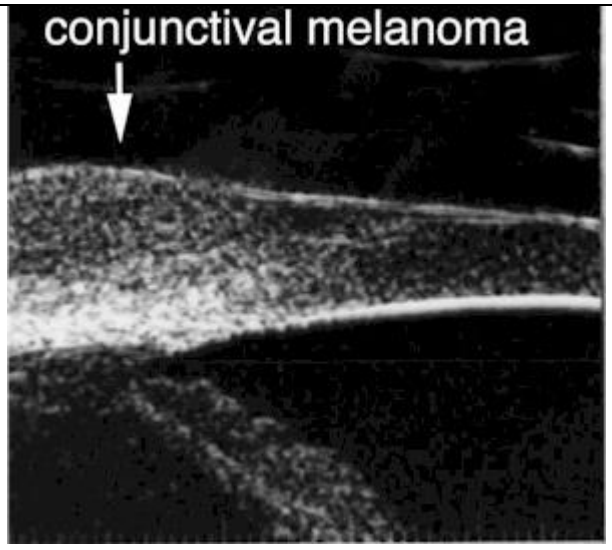

(figure 22) An example of uses of UBM showing conjunctival melanoma
Atlas Pavlin 1999-2000.

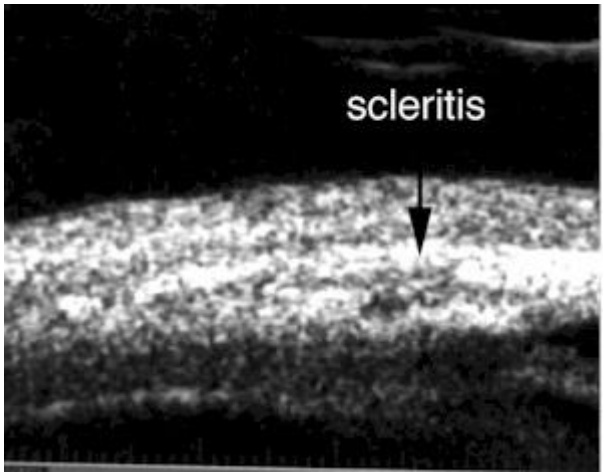

(figure 23) An example of uses of UBM showing a diseased sclera. The arrow showing scleritis. Atlas Pavlin 1999-2000

(figure 24) An example of uses of UBM the arrow showing a haptic of an IOL in bag
Atlas Pavlin 1999-2000.

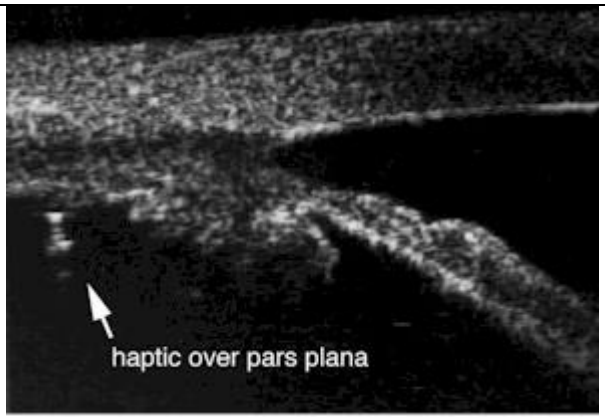

(figure 25) An example of uses of UBM the arrow showing a hptic over pars plana
Atlas Pavlin 1999-2000.

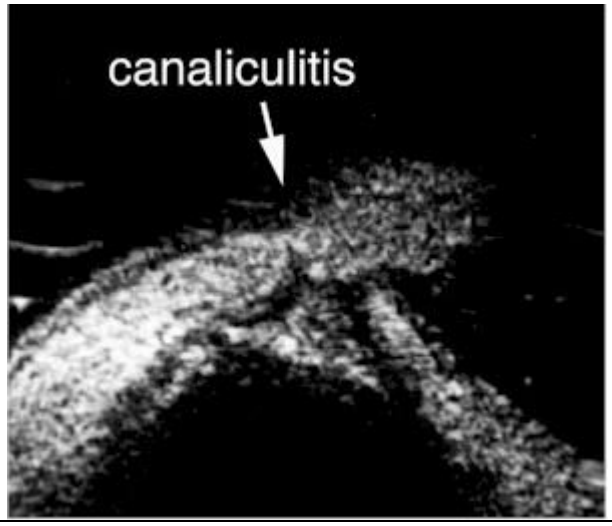

(figure 26) An example of uses of UBM the arrow showing canliculitis
Atlas Pavlin 1999-2000.

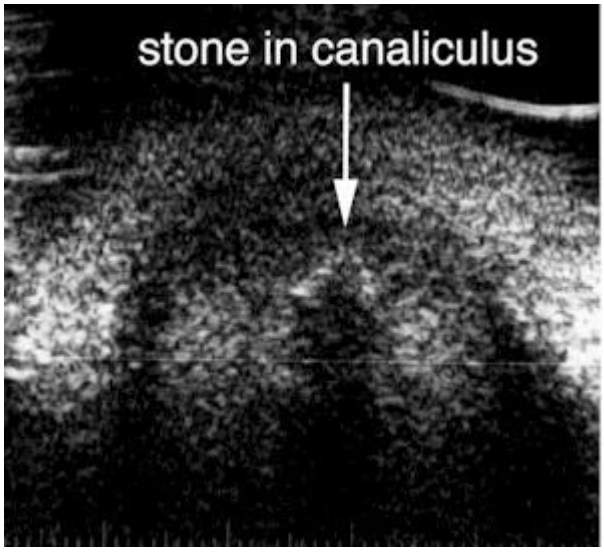

(figure 27) An example of uses of UBM the arrow showing a stone in the canaliculus
Atlas Pavlin 1999-2000.

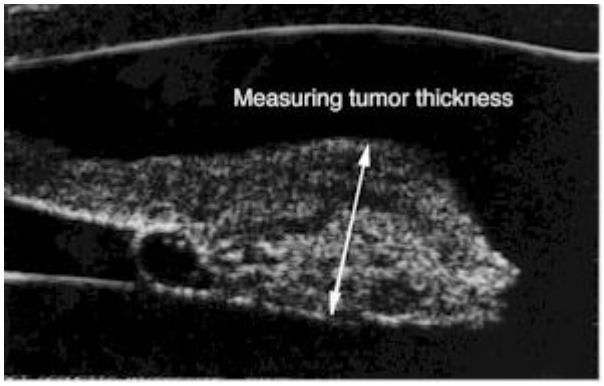

(figure 28) An example of uses of UBM the arrow showing a tumour measuring its thickness by the UBM
Atlas Pavlin 1999-2000.

Optical Coherence Tomography Of Anterior Segment

Since optical coherence tomography (OCT) was introduced as a new imaging method in ophthalmology, many studies have been published on OCT investigations of the posterior segment of the eye. However, OCT can also be an useful tool in examining the anterior segment of the eye at microscopic resolution. It can be helpful to image and measure complex details of corneal pathologies and structural changes of the chamber angle and the iris (Fujimoto et al., 1995).

The ability to define the relationship of angle structures in cross section allows a new morphometric gonioscopy and imaging of these structures at high resolution. Corneal thickness measurements by OCT can provide therapeutic control in refractive laser surgery. Since the commercially available OCT-system is fundus camera based, it does not allow routine examinations of the anterior segment. Therefore only a few experimental studies of OCT measurements of the anterior segment are published (Koop et al., 1997).

High two-dimensional resolution and excellent sensitivity have been demonstrated. To use examination techniques familiar to ophthalmologists, the OCT was adapted to a slitlamp, which allows comfortable and rapid measurements in routine clinical use of the anterior segment (Hoerauf et al.,1999).

Methods:

The images were generated by a newly developed slitlamp-adapted OCT-system. The potential and limitations of this technique as a diagnostic and biometric tool for measurements of the anterior segment in healthy subjects and in patients with pathologic changes are demonstrated.

Cornea Imaging:

The slitlamp-adapted OCT-system is capable to differentiate three corneal layers. The highest reflectivity is found at the epithelial-Bowman layer and at the Descemet-endothelial layer, whereas lower reflectivity is observed in the corneal stroma (Izatt et al.,1994).

It is not possible to differentiate between the epithelium and Bowman's membrane, or Descemet's membrane and the endothelium. In the corneo-scleral junction the different arrangement of the collagen fibres in cornea and sclera is responsible for the different optical properties in the two adjacent tissues with a dramatic change of reflectivity (Toth et al.,1997).

Conjunctiva, tenons, and sclera appear as only one highly reflective complex due to the highly scattering sclera, which limits OCT-imaging of deeper structures (Toth et al.,1997).

Pachymetric Analysis And Photorefractive Laser Surgery:

Photorefractive laser surgery has been proven successful to correct myopia, hyperopia and astigmatism in the last years. An exact corneal thickness measurement prior to the refractive ablation is the basis to avoid over- or under-correction. OCT offers the possibility to perform two-dimensional morphometric measurements of the cornea (Puliafito et al.,1996).

Scanning the incident beam perpendicular to the surface of the cornea results in a central specular reflection in the OCT-image. On the other hand, off axis reflectivity drops rapidly. To measure the corneal thickness precisely, the OCT beam was directed perpendicularly to the corneal surface (Wilkins et al.,1996).

Calibration was performed with a glass plate of defined thickness (148mm). The achievable precision of the central pachymetry is less than 3 microns. The optical path through the cornea was defined as the distance between the endothelial and epithelial maximum of the axial profile. The geometric thickness of the cornea equals the optical path length divided by

the group-refractive index of the cornea, which was assumed to be 1.376 (Snell et al.,1989).

Measurements were performed in the center of the cornea, the diameter of the scanning beam waist was 20 microns. The center of the pupil was taken as reference. Preliminary results of corneal thickness OCT-measurements showed a good agreement with ultrasonic pachymetry. The median central corneal thickness measured by OCT and ultrasonic pachymetry was 540 microns and 546 microns respectively. The median difference was only 6 microns, which corresponds to a systematic

underestimation with the corneal OCT of 1.2%. The double standard deviation of corneal thickness was 22 microns, which resulted in an error (2SD/xmean) of 4.1% (DiCarlo et al., 1995).

Photorefractive Keratectomy (PRK):

Pachymetric analysis during photorefractive laser therapy by OCT may improve the results of photorefractive laser therapy. OCT-measurements demonstrated thinning of the cornea after removal of the epithelium and photorefractive excimer laser keratectomy (PRK) in myopic patients (Hee et al., 1998).

The amount of the ablation thickness could be quantified reproducibly by calculating the difference of pre- and postoperative measurements. In myopic patients a flattening of the corneal profile could be observed after PRK. By spherical fitting of the surface profile measured by OCT before and after PRK the change in corneal refraction (D) can be calculated using the formula D/dpt = 337.5 (microns/R0 - microns/R1); with R0 and R1 being the radius of curvature before and after PRK respectively (Huebscher et al.,1996).

A limiting factor for the accuracy of corneal thickness measurements by OCT is the assumption of a constant refractive index of the human cornea before and after treatment(Hee et al., 1998).

Interestingly the contrast between corneal epithelium and stroma improves after PRK because of the slight haze, which means an increased opacity of the corneal stroma due to the wound healing process. Strong haze formation can be responsible for limited results in photorefractive laser treatment causing glare particularly at night. It can occur centrally, sectorally or arcuately and the risk of haze increases with the thickness of cornea ablated (Koop et al.,1997).

OCT may improve the investigation and quantitation of haze and haze-formation. Future studies by OCT should analyze the posterior corneal surface as well, to improve diagnosis of corneal changes such as corneal ectasia induced by PRK (Huebscher et al.,1996).

LASIK:

Another alternative approach in photorefractive laser treatment is Laser In-Situ Keratomileusis (LASIK). During this procedure a thin corneal flap is created by a microkeratome and the corneal stroma is treated by an excimer laser. OCT could allow a non-contact in vivo control of the thickness of these corneal flaps during LASIK.LTK (Laser Thermokeratoplasty) (Rutledge et al.,1996).

A third refractive laser treatment is the laser thermokeratoplasty (LTK), which was performed earlier by pulsed HolmiumYAG lasers and replaced later by a cw-infrared diode laser. In this treatment precise coagulation of the peripheral corneal stroma leads to a refractive correction. OCT is able to determine the location and the exact extent of this lesions as shown in this image of a patient after treatment by LTK for hyperopia (Fujimoto et al.,1995).

A precise biometric evaluation and documentation of the lesions and their dimensions is possible by OCT. The thermal LTK-effects are highly reflective and extend through almost the entire cornea nearly reaching the endothelial cell layer. Koop et al. compared morphological changes of the cornea measured by OCT with histological sections in enucleated porcine eyes after laser thermokeratoplasty and showed that OCT is able to deliver additional information without artificial changes caused by histologic preparation. He concluded that OCT may be able to provide an online control of the LTK parameters to improve the postoperative results and to avoid under- or over correction.

Corneal OCT Summary:

This indicate that the slitlamp-adapted OCT-system could become an important tool to improve and control photorefractive laser treatment, and may offer the possibility to give new information about corneal wound healing after these procedures. OCT may also be able to deliver more information about wound healing processes in the cornea after phototherapeutic keratectomy (PTK) which is performed in patients with recurrent epithelial defects or pterygium, which resembles fibrovascular tissue arising from the conjunctiva extending onto the cornea (Izatt et al.,1994).

With the existing OCT-system it is also possible to perform topographical measurements of the cornea, analyze corneal curvature and calculate corneal refraction. Limiting factors for corneal topography at the moment are the relatively long acquisition time for multiple images with resulting motion artifacts, often caused by patients' poor compliance, oculomotor dysfunction, or by reduced fixation. Further technical developments should aim to overcome these problems (Hee et al., 1998).

Iris:

OCT can resolve the iris into three different layers, a highly reflective thick superficial layer, a lower reflective stroma, and a thin highly reflective posterior layer of iris pigment epithelium (Chylack et al.,1993).

Changes in the superficial layers and in the configuration of the iris could be evaluated precisely as demonstrated in a patient with an anterior synechia (Chylack et al.,1993).

Other interesting ocular structures, which are clinically hardly or not observable like the ciliary body, the zonular fibers located at the equator of the lens, the pars plicata and the pars plana were shadowed in OCT by the highly reflecting iris pigment epithelium, attenuating the incident light of a 830nm light source. However changes within the iris such as iris cysts and iris tumors can be visualized, monitored and documented objectively to measure their size and control their possible growth (Hoerauf et al.,2000).

Anterior Chamber Angle:

The width of the anterior chamber angle is an interesting value, because it determines the risk for acute angle closure glaucoma. Also structural changes in the chamber angle, like fibrotic scar formation, or new vessel growth can cause a raise in intraocular pressure and may be detected earlier by OCT. Clinical examination and classification of the chamber angle is routinely performed by direct visualization using a gonioscopy lens. The classification according to Shaffer or Spaeth is widely used, but depends on the experience and the estimation of the individual examiner (Becker et al., 1972).

It is often difficult, if not impossible, to quantitatively compare follow up examinations in glaucoma patients. Hence, there is a need for an objective method to measure and document the chamber angle pre- and post-treatment

as seen in a patient after Nd:YAG-Laser-iridotomy with postoperative deepening of the anterior chamber (Pavlin et al.,1991).

By the slitlamp-adapted OCT the chamber angle could be visualized without using a gonioscopy lens and was demonstrated in high resolution cross section images. This OCT-system is an ideal device for the morphometry of the chamber angle in vivo similar to histologic sections but without artificial changes. OCT-images can be taken in each position and it seems reasonable to measure the angle at the 3, 6, 9 and 12 o´clock position (Hoerauf et al.,1999).

The ability of the OCT to show the angle region in cross-section allows quantitative measurements. However, due to the curvature of the cornea it is not possible to get a perpendicular incident light beam over the whole scanning range. The OCT-beam is refracted by the air-cornea interface if the incident angle of the beam is not perpendicular. To correct this refraction, the knowledge of the refractive index, the corneal curvature and the distance of the cornea to the iris is needed. In the presented OCT-system it was difficult to acquire the information because of the limited axial image depth of 2 mm (Schuman et al.,1994).

One more general limitation of this method so far is, that the peripheral part of the iris and the anterior chamber angle region, essential for classification of the chamber angle, are shadowed by the anteriorly located highly backscattering part of the sclera. To overcome this problem measurements were performed in oblique incident angles. If the incident OCT-beam was directed more obliquely, the chamber angle could be visualized completely, but the resulting distortion of the OCT images made it more difficult to quantify the chamber angle. Another drawback is that structures like the trabecular meshwork, as well as Schlemm's canal could not be identified because of shadowing properties of the anterior sclera (Puliafito et al.,1996).

Transscleral OCT:

To penetrate highly reflective tissues, like the sclera, the scleral spur, the iris pigment epithelium or hazy media such as corneal opacification, light sources with a wavelength longer than 830nm could be useful. OCT-images generated by an experimental prototype using an handheld applicator for

dermatological examinations and a superluminiscent diode emitting at a wavelength of 1310nm were promising (Fujimoto et al.,1995).

The number of lateral scans varied between 100 and 400. In enucleated pig and human eyes the chamber angle could be fully visualized without shadowing by the anterior part of the sclera. Furthermore the ciliary body could be identified. By the use of a 1310nm light source the scleral-choroidal-retinal complex could be demonstrated. With a slitlamp-adapted prototype also in-vivo measurements of the anterior chamber angle and the ciliary body could be performed successfully (Hee et al.,1998).

The technique provides an excellent resolution but a limited penetration depth which makes an exact evaluation of the ciliary body area difficult. A further increase of the wavelength may improve the visualization of this region (Hee et al.,1998).

Normal Lens And Cataract:

OCT-imaging of the lens, capsular bag as well as anterior vitreous was possible within the pupillary opening. OCT-measurements of the human lens in a young healthy adult revealed a slightly increased reflectivity in the nuclear region and the lens capsule (Chylack et al.,1993).

In patients with a nuclear cataract, the lens nucleus revealed a markedly higher reflectivity than the cortex. Due to the limited lateral depth of 2mm, the whole thickness of the lens could not be visualized in one OCT-image. Combining several OCT-images measurement of the lens thickness was possible (DiCarlo et al.,1995).

The slitlamp-adapted OCT can serve as an important diagnostic tool by densitometric analyses of the human lens, correlating the reflectivity of lens opacities to morphologic changes. This may offer an objective classification and new grading system for cataract development which otherwise is only possible with the Scheimpflug camera system or with a subjective method, the LOCS III-test (Huebscher et al.,1996).

This test is a classification system based on a set of standard color photographic transparencies of cataract, that can be used as references to classify lens opacities at the slit-lamp. In a cataract model OCT was able to detect induced nuclear cataracts in enucleated calf eyes. First experimental

in-vivo measurements in monkeys were performed by DiCarlo et al., who converted the reflectivity to a qualitative grading system and correlated the results with the LOCS III-test .

Intraocular Lenses And Secondary Cataract:

The capsular bag, particularly if secondary cataract formation was present, could be visualized as a well-defined slightly hyperreflective bandlike structure by OCT in-vivo (Koop et al.,1997).

Reflectivity of the bag increased with the thickness of secondary cataract formation, and could be quantified by OCT. Also the anterior vitreous could be examined by the slitlamp-adapted OCT-system (Koop et al.,1997).

OCT-measurements of lens, secondary cataract, and anterior vitreous are only possible within the pupillary opening and are very limited in eyes with small pupils. We examined patients with intraocular lenses of the three different materials, PMMA-, acrylic- and silicone, which are the most common used today in cataract surgery. The capsular bag could be identified, however in no case could the intraocular lens itself could be visualized by OCT. The reason for this phenomenon is probably the homogenous and extremely translucent material of the lenses and their smooth surface. Therefore only a punctual specular reflection could be detected but no structure could be visualized within the OCT-image (Hoerauf et al.,1999).

Potential And Limitations Of Oct In The Anterior Segment:

Imaging in ophthalmology has considerably improved over the past years, but only selected techniques allow high resolution imaging of the anterior segment. The first clinical experiences of the slitlamp-adapted OCT-system, which was developed for routine clinical examinations of the anterior and posterior segment, are promising (Wilkins et al.,1996).

OCT-measurements performed with this system deliver high resolution cross-sectional images of intraocular structures using the familiar slitlamp examination technique, thus, extending the use of OCT to the anterior globe. It allows a quick change between anterior and posterior segment examinations and provides exact and rapid biometric analyses of structures

and dimensions in the anterior globe without direct contact or immersion techniques (Izatt et al.,1994).

Important clinical measurements include corneal thickness, corneal surface profile and corneal refraction, iris thickness, anterior chamber angle, lens thickness, and thickness of secondary cataract formation. A drawback is that direct morphometric analysis are only possible for axial measurements. Off-axis measurements need further correction. For this correction, the knowledge of the profile of the ocular structures anteriorly to the structure of interest is required (Toth et al.,1997).

Perspectives:

There is a wide range of potential clinical and scientific applications for the presented slitlamp-adapted OCT-system in the anterior segment of the eye. Further technical improvements will shorten the acquisition time and reduce motion artifacts. Optimization of the coherence signal demodulation and image processing can improve sensitivity and contrast of the OCT-images. An increased length of the lateral scan will provide a better analysis of the complete anterior segment. A simultaneous documentation of the scanned area in related color photographs will further improve the reproducibility of measurements and orientation within the images. Future studies will have to investigate especially the infrared OCT-technique which has the potential to replace ultrasound biomicroscopy. Current technical refinements and the slitlamp-adaption of this OCT will improve the quality for the examination of the anterior segment of the eye (Hoerauf et al.,2000).

(figure 32) Slitlamp-adapted OCTsystem Prototype of the slitlamp adapted OCT-system. The scanning module is integrated in a Haag-Streit (BQ 900) slitlamp (arrow).

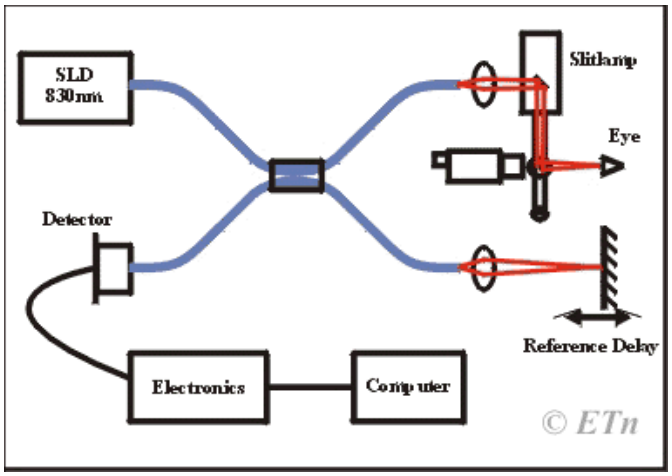

(figure 33) Schematic diagram of the slitlamp-adapted OCT

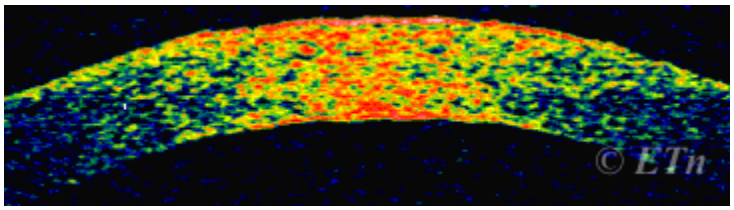

(figure 34) Scaled OCT-image of a healthy human cornea in vivo with higher reflectivity of the epithelium and the endothelium, and lower reflectivity in the corneal stroma. The higher signal in the central area is caused by the perpendicular angle of the OCT-beam to the arrangement of the collagen fibres in the cornea (100 Hz scanning rate, 200 axial scans, 5.5 x 2 mm).

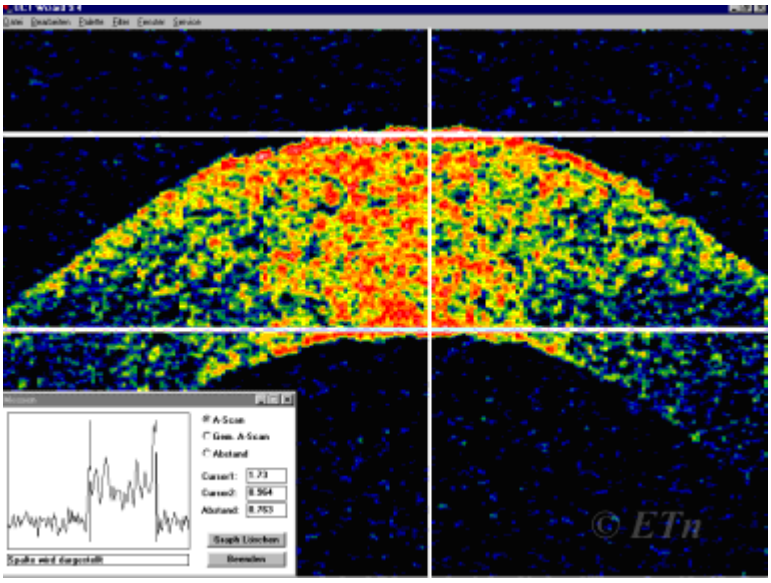

(figure 35) Pachymetric measurement of a healthy human cornea in vivo showed an optical path of 776 mm, which results in a corneal thickness of 562 mm considering a refractive index of 1.38 (100 Hz, 200 scans, 5.5 x 2 mm).

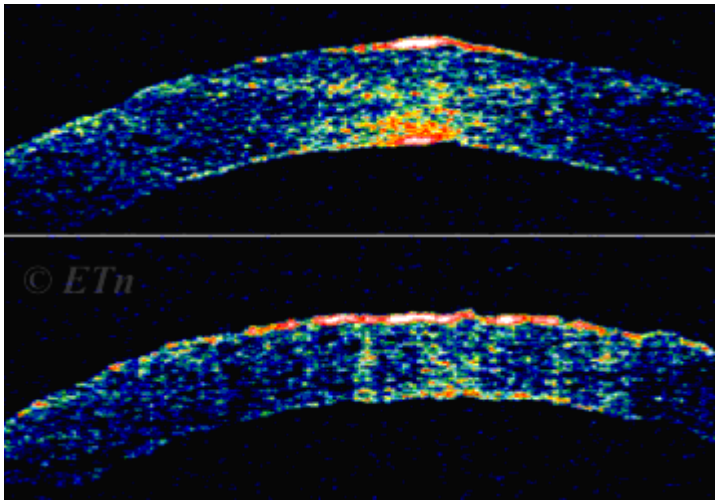

(figure 36) Corneal OCT before and after PRK in a myopic patient (-5.5dpt) showing corneal thinning and flattening after treatment. Image

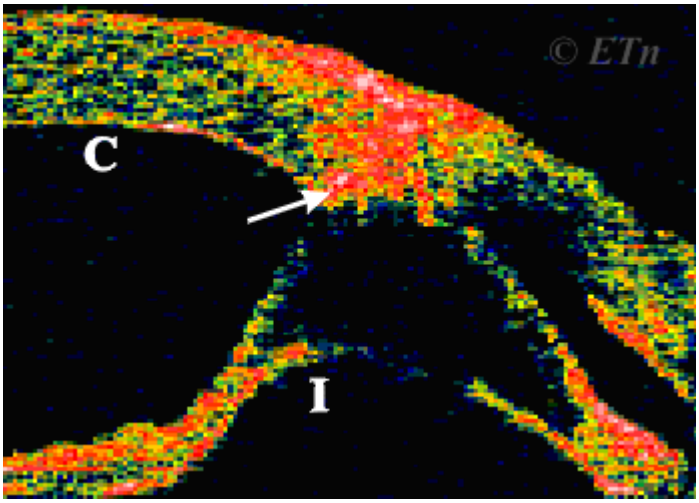

(figure 37) Patient after perforating eye injury with an anterior synechia (arrow) and separation of the iris layers (Cornea = C, Iris = I). This is one of the first images and was performed with 54 Hz showing 100 lateral scans resulting in a reduced resolution (5.5 x 2 mm).

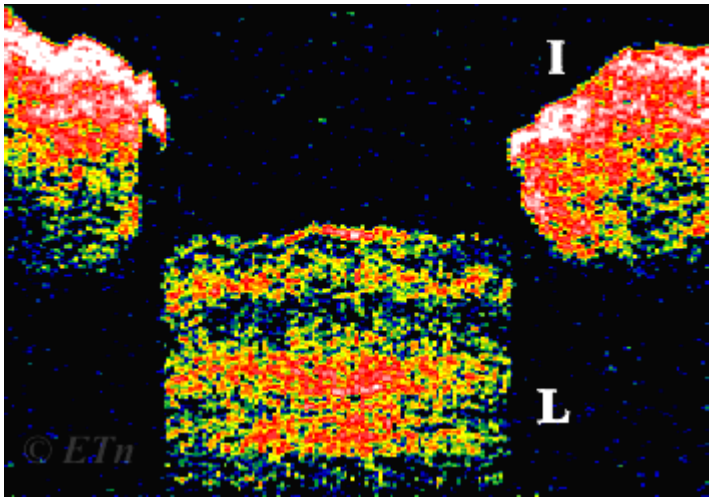

(figure 38) OCT of iris (I) and lens (L) in a healthy young patient in miosis. The highly reflective iris is shadowing structures located posterior to it. The lens capsule and nuclear region shows a higher reflectivity, whereas the cortex is hyporeflective (100 Hz, 200 scans, 5.5 x 2 mm).

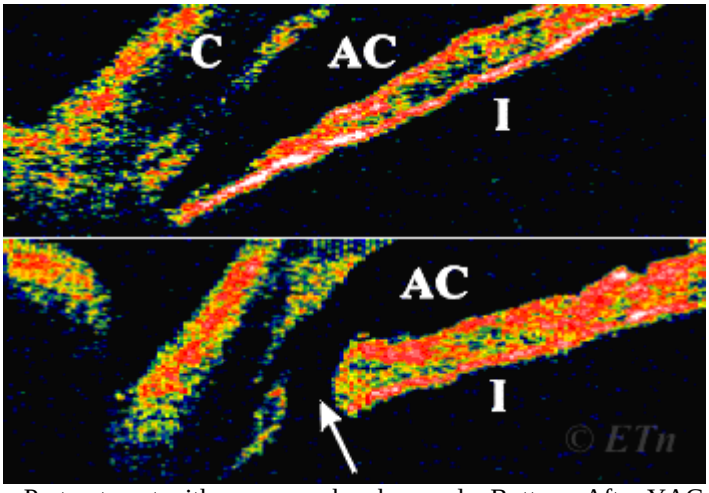

(figure 39) Top: Pretreatment with a narrow chamber angle. Bottom: After YAG iridotomy with demonstration of the opening in the iris (arrow) and deepening of the anterior chamber.

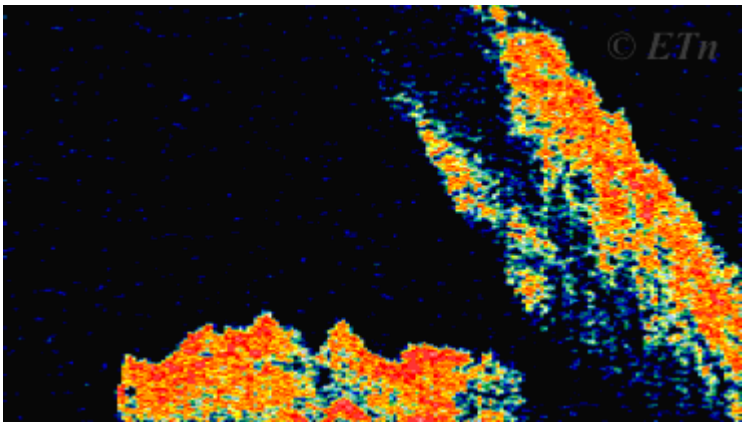

(figure 40) OCT-image (100 Hz, 200 scans, 5.5 x 2 mm) of an open chamber angle and corneoscleral region. Shadowing of the most peripheral part of the angle and iris by the highly backscattering anterior part of the sclera.

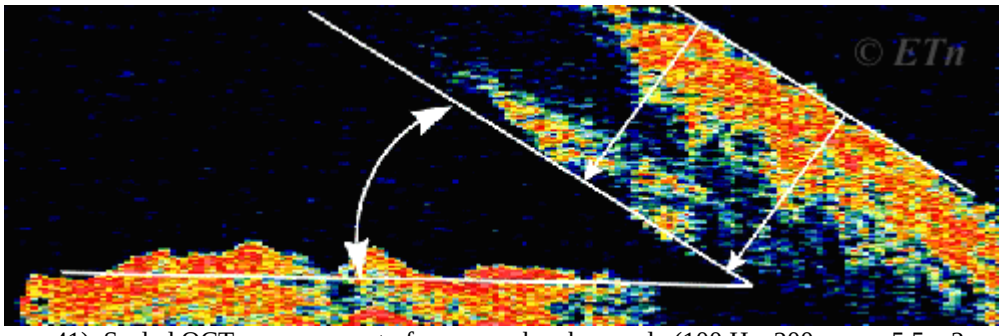

(figure 41) Scaled OCT-measurement of an open chamber angle (100 Hz, 200 scans, 5.5 x 2 mm). Limitations are the missing reference point due to shadowing of the peripheral iris and the uneven iris configuration. The refraction causes distortion in the OCT-image, thus, quantitative measurements require mathematical correction (Iris = I, Cornea = C).

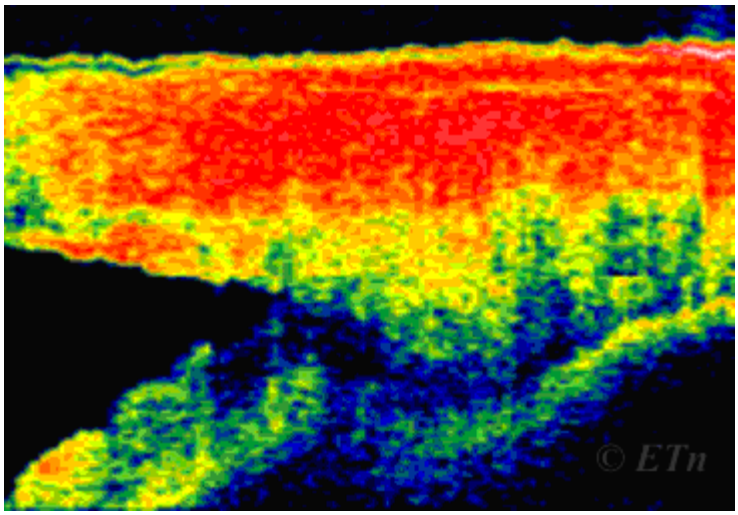

(figure 42) In-vivo transscleral OCT-measurement in a healthy human eye with a prototype of a 1310nm OCT allowing complete visualization of the chamber angle.

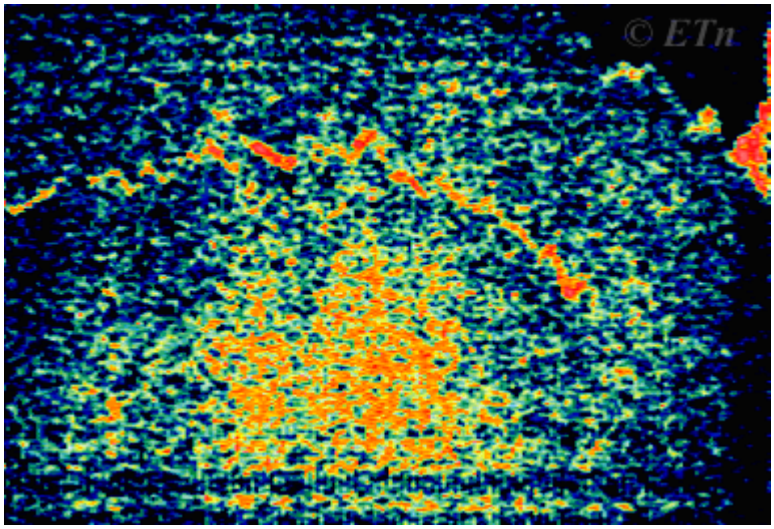

(figure 43) OCT-image of a senile nuclear cataract. The lens nucleus (N) was corresponding to a higher reflectivity and appeared well demarcated in the OCT, whereas the lens cortex is hyporeflective (100 Hz, 200 scans, 5.5 x 2 mm).

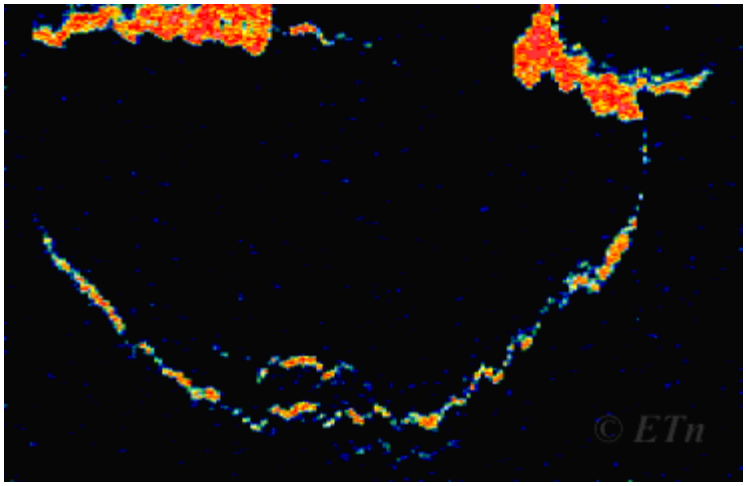

(figure 44) OCT image of a pseudophakic patient with secondary cataract formation. Capsular bag showed hyperreflectivity of the anterior (A) and posterior (P) capsular opacification in the OCT; the intraocular lens could not be visualized.

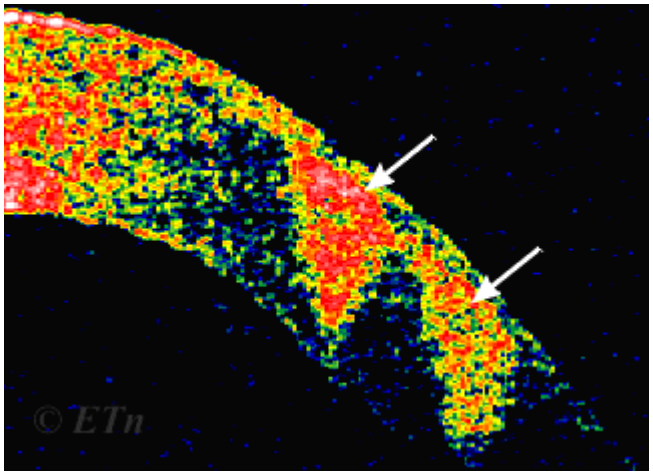

(figure 45) Slitlamp-adapted OCT allowed visualization of laser effects in the cornea in a patient one week after Ho-Laser thermokeratoplasty. The laser effects (arrows) are hyperreflective and extend through almost the whole of corneal thickness nearly reaching the endothelium (100 Hz, 200 scans, 5.5 x 2 mm).

Summary

Recent anterior segment imaging techniques are developing rapidly. From these recent techniques: Slit lamp photography, Corneal Topography, Specular Microscopy, Fluorophotometry, Ultrasound biomicroscopy and Optical Coherence Tomography.

The slit lamp is a special microscope that provides a magnified, three-dimensional view of the different parts of the eye. Recently assessment of the anterior segment is performed using a slit lamp video imaging system.

Corneal topography is a method of measuring and quantifying the shape and the curvature of the corneal surface. Which is developing rapidly, mainly because of recent advances in refractive surgery.

Specular microscopy is a photographic test used to visualize the human endothelium. There are 2 types of specular microscopy: contact and non contact microscopy. To determine endothelial cell density, contact and noncontact specular microscopy may be used interchangeably.

Ocular Fluorophotometry techniques is one of the most popular imaging are based on modification of standard slit lamp photographic techniques. With a slit lamp fluorophotometric technique is limited to anterior segment to monitor corneal and lens fluorescence.

Ultrasound Biomicroscoy (UBM) differentiated well The corneal layers. The corneoscleral junction can be distinguished consistently with UBM. The scleral spur is a very useful landmark presenting a constant reference point for measurement in the angle of the anterior chamber. The iris is well imaged in cross section by UBM.

Optical coherence tomography(OCT) permits high resolution cross-sectional imaging of biological tissue using light. OCT is a technology for non-contact imaging of transparent and scattering media. OCT has the advantage of being non-contact comfortable and well tolerated by the patient.

References

-A-

Abbott R, Forster R. Clinical specular microscopy and intraocular surgery. Arch Ophthalmol. 1979;97:1476.

Amsler M: Kératocône classique et kératocône fruste; arguments unitaires. Ophthalmologica 1946; 111.96-710.

Anderson DR, Jin JC, Wright MM: the physiological characteristics of relative papillary block. Am J Ophthalmology 1991; 111-344.

Auffarth GU, Tetz MR, Biazid Y, et al. Measuring anterior chamber depth with the Orbscan topography system. J Cataract Refract Surg 1997;23:1351-1355.

Augusburger JJ, Affel LL, Benaro SH: UBM of cystic lesion of the iris. Trans Am. Ophthalmology. Soc. 1996; 94: 259-74.

Avitabile T, Russo V, Sorce MC: A new apparatus for the study of anterior segment disorders: The UBM; in Cennamo Grand Rosa N: Ultrasonography in ophthalmology. Dordrecht, Kluwer Academic Publishers 1997; vol 15, pp 155-62.

Avitabile T, Russo V, Girlanda R, Marino A: Corneal Oedema: diagnosis and surgical planning with UBM. Ophthalmologica 1998; 212 (1): 13-16.

Avitabile T, Marano F, Castiglion F: keratoconus staging with UBM. Ophthalmologica 1998; 212 : 10-12.

Awan KJ: Peters-Reiger's syndrome J Pediatric Ophthalmol 1977; 14: 112-16.

-B-

Becker SC (1972) Gonioscopic grading of the angle. In: Becker S C (ed) Clinical Gonioscopy. A text and stereoscopic atlas. Mosby, St. Louis, pp 73-80.

Belin MW, Litoff D, Strods SJ, et al. The PAR technology corneal topography system. Refract Corneal Surg 1992;**8**:88-896.
Bessho K, Sawada A, Yamanoto T: A case of Peters' anomaly observed by UBM. Jab J Clin Ophthalmol 1998; 52:215-18.

Bhende M, Agraham SG, Gobal L: UBM of sclerotomy sites after pars plana vitrectomy. Ophthalmology 2000; 107:1729-36.

Binder PS. Videokeratography. CLAO J 1995;**21**:133-144.

Bocker T and Spiznas M: UBM for examination of the sclerotomy site after vitrectomy. Am J Ophthalmology 1999; 118:813-15.

Bogan SJ, Waring GO III, Ibrahim O, *et al*. Classification of normal corneal topography based on computer-assisted videokeratography. Arch Ophthalmol 1990;**108**:945-949.

Bourne W, Kaufman H. The endothelium of clear corneal transplants. Arch Ophthalmol. 1976;94:1730.

Bovelle R, Kaufman S, Thompson H, Hamano H. Corneal thickness measurements with the Topcon SP-2000P specular microscope and an ultrasound pachymeter. Arch Ophthalmol. 1999;117:868-70.

Bron AJ: Keratoconus. Cornea 1988; 7:163-9.

Brooks A, Grant G, and Gillies W. Differentiation of posterior polymorphous dystrophy from other posterior corneal opacities by specular microscopy. Ophthalomology. 1989;96:1639.

Brown LF: Ferroelectric polymers: Current and future application. IEEE ultrasonic symposium proceedings 1992, pp 539- 545.

Byrne SF and Green RL: Ultrasound of the eye and orbit. St Louis Mosby-Year Book 1992; ch 1 physics and instrumentation:1-15.

Byrne SF, Green RL (eds): Axial Eye Length Measurements (A-Scan Biometry) in Ultrasound of the Eye and Orbit. St. Louis, Mosby, Second Edition, 2002.

-C-

Carassa RG, Betten P,Fiori M: Nd: YAG laser iridotomy in pigment dispersion syndrome. Br J Ophthalmology 1998;82:150-53.

Caronia RM, Leibmann J, Stigman Z: increase in iris-lens contact after laser iridotomy. Am J Ophthalmology 1996; 122:53-57.

Carr J, Thompson K, Stulting R, Waring G: LASIK: Emory Vision Correction Center. In: The Art of Lasik. 2nd ed. 2000: 281-92.

Chako JG, Figueroa RE, Johnson MH, *et al*. Detection and localisation of steel intraocular foreign bodies using computed tomography—a comparison of helical and conventional axial scanning. *Ophthalmology* 1997;**104**:319-323.

Chylack LT, Wolfe JK, Singer DM, Leske C, Bullimore MA, Bailey IL, Friend J, McCarthy D, Suh-Yuh W (1993) The lens opacities classification system III. Arch Ophthalmol 111:831-836.

Cormier G, Brunette I, Boisjoly HM: Anterior stromal punctures for bullous keratopathy. Arch Ophthalmol 1996 Jun; 114(6): 654-8.

-D-

Darrel L. Conger, CRA October 2000.

DiCarlo CD, Boppart S, Gagliano DA, Amnotte R, Smith AB, Hammer DX, Cox AB, Hee MR, Fujimoto J, Swanson E, Roach WP. (1995) A new

noninvasive imaging technique for cataract evaluation in the rheus monkey. In: Proceedings of Lasers in Surgery: Advanced characterization, therapeutics, and systems V. SPIE Volume 2395, 636-643.

-E-

Edmund C. Posterior corneal curvature and its influence on corneal dioptric power. Acta Ophthalmol (Copenh) 1994;**72**:715-720.

Eiferman RA: Association of Wilm's tumor with Peters' anomaly. Ann Ophthalmol 1984; 933-4.

Esaki K, Ishikawa H, Leibmann JM: A technique for performing UBM in the setting and prone positions. Ophthalmic Surg Laser 2000;31: 166-9.

-F-

Falcinelli GC, Avitabile T, Cilliardo P: the usefulness of echography before and after osteo-odonto-kerato-prosthesis in Cennamo Grand Rosa N: : Ultrasonography in ophthalmology. Dordrecht, Kluwer Academic Publishers 1997; vol 15, pp 201-5.

Feijoo JG, Carbajo MM, Banitllo Jm: Orbital cup. Arch Ophthalmol. 1997; 115: 1475-76.

Fong LP, Sainz DM, Rice BA: immunopathology of scleritis. Ophthalmology 1991; 98:472-9.

Foster FS, Strban M, Austin G: the ultrasonic macroscope. Ultrasonic imaging 1984; 6:243-61.

Fujimoto JG, Brezinski ME, Tearney GJ, Boppart SA, Bouma B, Hee MR, Southern JF, Swanson EA (1995) Optical biopsy and imaging using optical coherence tomography. Nature Med 1:970-972.

-G-

Gills JP et al: Corneal topography: The state of the art. Slack Incorporated; 1995: 1-328.

Grant CA and Azar D: UBM in the diagnosis of limbal dermoid. Am J Ophthalmology 1999; 128: 365-67.

-H-

Haamann P, Jensen OM, Schmidt P: Changing indications for penetrating keratoplasty. Acta Ophthalmol (Copenh) 1994 Aug; 72(4): 443-6.

Hara, Makiko MD; Morishige, Naoyuki MD, PhD; Chikama, Tai-ichiro MD, PhD; Nishida, Teruo MD, DSc Cornea. 22(6):512-515, August 2003.

Haddad AM, Greenfield DS, Stigman Z: Peters' anomaly: diagnosis by UBM. Am J Ophthalmology 1997; 28:311-12.

Hee MR, Puliafito CA, Duker JS, Reichel E, Coker JG, Wilkins JR, Schuman JS, Swanson EA, Fujimoto JG (1998) Topography of diabetic macular edema with optical coherence tomography. Ophthalmology 105:360-370.

Heiligenhaus A, Schilling M, Lung E: UBM in scleritis. 1998; 105:527-34.

Herndon LW, Choudhri SA, Cox T, *et al*. Central corneal thickness in normal, glaucomatous, and ocular hypertensive eyes. Arch Ophthalmol 1997;**115**:1137-1141

Hetherington J, Jr. The spectrum of Chandler's syndrome. Ophthalmology. 1978;85:240.

Hirst L, Quigley H, Stark W, Shields M. Specular microscopy of iridocorneal endothelial syndrome. Amer J Ophthalmol. 1980;89:11.

Hirst L, Green W, Luckenback M, Cruz Z, Stark W. Epithelial characteristics of the endothelium in Chandler's syndrome. Inv Ophthalmol Vis Sci. 1983;24:603.

Hitzenberger CK, Baumgartner A, Drexler W, et al. Interferometric measurement of corneal thickness with micrometer precision. Am J Ophthalmol 1994;118:468-476.

Hoerauf H, Wirbelauer C, Scholz C, Engelhardt R Koch P, Laqua H, Birngruber R (1999) Slitlamp-adapted optical coherence tomography (OCT) of the anterior segment. Graefe´s Arch Clin Exp Ophthalmol in press.

Hoerauf H, Gordes RS, Scholz C, Wirbelauer C, Koch P, Engelhardt R, Winkler J, Laqua H, Birngruber R (2000) First experimental and clinical results with transscleral optical coherence tomography. Ophthalmic Surg Lasers 31:218-222.

Hoffer K, Kraft M. Normal endothelial cell count range. *Ophthalmology*. 1980;87:861.

Holladay JT: Corneal topography using the Holladay Diagnostic Summary. J Cataract Refract Surg 1997 Mar; 23(2): 209-21.

Hudde T, Althaus C, Sundmacher: postoperative UBM evaluation of the haptic position in transsclerally sutured posterior chamber lens. Ger J Ophthalmology 1996; 5:449-53.

Huebscher HJ, Genth U, Seiler T (1996) Determination of excimer laser ablation rate of the human cornea using in vivo Scheimpflug videography. Invest Ophthalmol Vis Sci 37-42.

-I-

Irene ME, Landau, Laurell CG: UBM evaluation of intraocular lens haptic position after phacoemulsification with curvilinear continuous capsulorhexis. Acta. Oph. Scand 1999; 77:394-96.

Izatt JA, Hee MR, Swanson EA, Lin CP, Huang D, Schuman JS, Puliafito CA, Fujimoto JG (1994) Micrometer-scale resolution imaging of the anterior

eye in vivo with optical coherence tomography. Arch Ophthalmol 112:1584-1589.

-J-

Jakus M. Further observations on the fine structure of the cornea. Invest Ophthalmol. 1962;1:202.

Joo CK, Kim TG: Corneal perforation during laser in situ keratomileusis. J Cataract Refract Surg 1999 Aug; 25(8): 1165-7.

-K-

K Kawana, T Tokunaga, K Miyata, F Okamoto, T Kiuchi, and T Oshika Comparison of corneal thickness measurements using Orbscan II, non-contact specular microscopy, and ultrasonic pachymetry in eyes after laser in situ keratomileusis. Br J Ophthalmol 2004; 88: 466-468.

Kanski JJ: Clinical ophthalmology asystematic approach (4th)edition; Butterworth-Heinemann 1999.

Kapetansky FM: A new water bath for UBM. Ophthalmic Surg. Laser. 1997; 28: 605-6.

Kaufman HE, Barron BA, McDonald M, Kaufman SC: Companion Handbook to the Cornea. Butterworth Heinemann; 2000: 947-59.

Kavickhoff JR: Response to Fourman Iridotomy in eyes with pigmentary glaucoma. Ophthalmic Surgery 1992; 23:843-44.

Kenyon KR: Mesenchymal diagnosis in Peters' anomaly. Exp Eye Res 1975; 21:125-42.

Kezirian G, Casebeer J: The CRS LASIK Study. In: The Art of Lasik. 2nd ed. 1999: 293-302.

Knorz MC, Wiesinger B, Liermann A, et al: Laser in situ keratomileusis for moderate and high myopia and myopic astigmatism. Ophthalmology 1998 May; 105(5): 932-40.

Koffler MC, Burlew JA: Corneal Topography and the Corneal Modeling System. Mediguide Ophthalmology 1991; 6: 1-5.

Koop N, Brinkmann R, Lankenau E, Flache S, Engelhardt R, Birngruber R (1997) Optische Kohrenztomographie der Kornea und des vorderen Augenabschnitts. Ophthalmologe 94:481-486.

Krachmer JH, Mannis JM, Holland EJ: Cornea. In: Mosby. 1997: 1-2253.

Kwok AKH, Tham CCY, Loo AVP: UBM of conventional and sutureless pars plana sclerotomies. Am J Ophthalmology 2001; 132: 172-77.

Kwon SI, Shin MC, Choi DG. The Evaluation of Anterior Segment Circulation after Strabismus Surgery by using Indocyanine Green(ICG) Iris Angiography. J Korean Ophthalmol Soc. 1998 Dec;39(12):3069-3077. Korean.

-L-

Laing R, Sandstrom M, Berrospi A, and Leibowitz H. The human corneal endothelium in keratoconus. A specular microscopic study. Arch Ophthalmol. 1979;97:1867.

Laing R, Leibowitz H, Chang R, Theodore J, Oak S. The endothelial mosaic in Fuchs dystrophy. A qualitative evaluation with specular microscope. Arch Ophthalmol. 1981;99:80.

Laing R, Neubauer L, Oak S, Kayne H, Leibowitz H. Evidence for mitosis in the adult corneal endothelium. Ophthalmol. 1984;10:1129.

Laganowski H, Sherrard E, and Kerr Muir M. The posterior corneal surface in posterior polymorphous dystrophy. A specular microscopical study. Cornea. 1991;10(3):224.

Laszlo Modes Jr., MD, PhD, Achim Langenbucher, PhD, Berthold Seitz, MD, EBOD J Cataract Refract Surg 2002; 28:1763–1769.
Lemp MA, Dilly PN, Boyde A. Tandem-scanning (confocal) microscopy of the full-thickness cornea. Cornea 1985;**4**:205-209.

Lezzi R, Rosen RB, Tello C: personel computer based three dimentional UBM of the anterior segment . Arch Ophthalmol 1996; 114: 520-24.

Liu Z, Huang AJ, Pflugfelder SC: Evaluation of corneal thickness and topography in normal eyes using the Orbscan corneal topography system. Br J Ophthalmol 1999 Jul; 83(7): 774-8.

-M-

Margio FA, Finger PT, Mc Cormek : Anterior segment implantation cyst Arch Ophthalmol 1998; 116: 1569-1575.

McWhae J, Willerschidt A, Gimbel H: UBM in refractive surgery. J. Cat. Ref. Surg. 1999; 20: 493-97.

Milner MS, Liebmann JM, Tello C: High resolution UBM of the anterior segment of the eye with dense corneal scar. Ophthalmic Surgery 1994; 25: 410-11.

Morinelli EN, Najac RD, Speacher MG: repair of Descemt's membrane detachment with the assistance of intraoperative UBM. Am J Ophthalmology 1996; 121: 718-72.

Murray DC, Potamitis T, Good P, Kirkby GR, Benson MT: Biometry of the silicone oil-filled eye. Eye. 2000 Feb;14 (Pt 1):118-20.

Murray D C, Durrani O M, Good P, Benson M T and Kirkby G R: Biometry of the silicone oil-filled eye: Eye (2002) 16, 727-730.

Musch D, Schwartz A, Fitzgerald-Shelton K, Sugar A, and Meyer R. The effect of allograft rejection after penetrating keratoplasty on central endothelial cell density. Am J Ophthalmol. 1991;111:739.

Myles WM, Flanders ME, Chitayat D: Peters' anomaly: a clinicopathologic study. J Pediatric Ophthalmol 1992; 29: 374-81.

-N-

Naufal SC, Hess JS, Friedlander MH, et al. Rasterstereography-based classification of normal corneas. J Cataract Refract Surg 1997;**23**:222-230.

Nischal KK, Naor J, Jay V: Clinicopathological correlation of congenital corneal opacification using UBM. British J Ophthalmology 2002; 86: 62-69.

Neubauer L, Laing R, Leibowitz H, Oak S. Coalescense of endothelial cells in the traumatized cornea. I: Experimental observation in cryopreserved tissue. Arch Ophthalmol. 1983;101:1787.

-O-

Ohya S, Nishimaki K, Nakayasu K, Kanai A. Department of Ophthalmology, School of Medicine, Juntendo University, Tokyo, JapanCLAO J. 1996 Apr;22(2):122-6.

-P-

Pande M, Hillman JS: Optical zone centration in keratorefractive surgery. Entrance pupil center, visual axis, coaxially sighted corneal reflex, or geometric corneal center? Ophthalmology 1993 Aug; 100(8): 1230-7.

Pavlin CJ, Harasiewicz K, Sherar MD, Foster FS (1991) Clinical use of ultrasound biomicroscopy. Ophthalmology 98:287-295.

Pavlin CJ, Harasiewicz K,Foster FS: Ultrasound biomicroscopy of anterior segment structures in normal and glaucomatous eyes. Am J of Ophthalmology 1992 Apr 15;113 (4): 381-9.

Pavlin CJ, Ritch R, Foster FS: UBM in plateau iris syndrome . Am J Ophthalmology 1992; 113: 390-95.

Pavlin CJ, Mc Whae JA, MC Gowan HD: UBM of anterior segment tumors. Ophthalmology 1992; 99: 1220-1228.

Pavlin CJ, Foster FS, Sherar MD: Ultrasound biomicroscopic assessment of anterior scleral diseases Am J Ophthalmology 1993; 116: 628-35.

Pavlin CJ, Foster FS, Harasiewicz K: UBM assessment of the cornea following excimer laser photokeratectomy. J Refract Surg 1994; 20:206-11.

Pavlin CJ, Foster FS: Ultrasound biomicroscopy of the eye. New York: springer-Verlag 1995.

Pavlin CJ, Foster FS: UBM high frequency ultrasound imaging of the eye at microscopic resolution. Radiol Clin North America 1998 Nov;36(6) :1046-58.

Peter Fedor, MD**,** Stephen C Kaufman, MD, PhD Corneal Topography and Imaging internet e-medicine February 2005.

Petroll WM, Roy P, Chuong CJ, et al. Measurement of surgically induced corneal deformations using three-dimensional confocal microscopy. Cornea 1996;15:154-164.

Potash SD, Tello C, Leibmann J: UBM in the pigment dispersion syndrome. Ophthalmology 1994; 101:332-339.

Presberg S, Quigley H, Foster R, Green W. Posterior polymorphous corneal dystrophy. Cornea. 1986;4:239.

Probst L, Hakim O, Nichols B, Baird M: LASIK Results from TLC, The London Laser Center. In: The Art of Lasik. 2nd ed. 1999: 303-8.

Puliafito CA, Hee MR, Schuman JS, Fujimoto JG (1996) Optical coherence tomography of ocular diseases. Slack Inc, Thorofare, NJ.

-R-

Rabbetts RB: Clinical Visual Optics. Butterworth Heinemann; 1998: 378-420.

Rao NA, Mark GE, Hidayat AA: necrotizing scleritis. A clinicopathological study of 41 cases Ophthalmology 1985; 92:1542.

Reinstein DZ, Silverman RH, Allemann N: High frequency ultrasound digital signal processing for Biometry of the cornea. Arch ophthalmology 1993; 111: 430-431.

Renee Bovelle, MD; Stephen C. Kaufman, MD, PhD; Hilary W. Thompson, PhD; Hikaru Hamano, MD Arch Ophthalmol. 1999;117:868-870.

Ritch R, Liebmann J, Lezzi R and Tello C: practical uses of Ultrsound Biomicroscopy in glaucoma. In: "Imaging in glaucoma ". Shuman JS (Ed.). Slack incorporated, NJ, USA, 1997; section 4, Ch. 10, Pp: 177-196.

Rutledge BK, Puliafito CA, Duker JS, Hee MR, Cox MS (1996) Optical coherence tomography of macular lesions associated with optic nerve head pits. Ophthalmology 103:1047-105.

Rutnin SS, Pavlin CJ, Solomovic AR: preoperative UBM assessment the ease of haptic removal before penetrating keratoplasty. Cat. Ref. Surg. 1997; 23: 239-43.

Ruusuvaara P. The fate of preserved and transplanted human corneal endothelium. Acta Ophthalmol. 1980;58:440.

-S-

Sachdev N, Cairns G, McGhee CNJ. . An introduction to wavefront aberrometry of the eye. NZ Optics May 2002, 12.

Salz JJ, Azen SP, Berstein J, et al. Evaluation and comparison of sources of variability in the measurement of corneal thickness with ultrasonic and optical pachymeters. Ophthalmic Surg 1983;14:750-754.

Schuman JS: Ophthalmic imaging and diagnostics. Ophthalmology Clinics of North America 1998; 11: 1-490.

Sherar MD, Starkoski BG, Foster FS: A 100 MHz B-scan ultrasound backscatter microscope. Ultrasonic imaging 1989; 11:95-105.

Sherrard E, Novakovic P, Speedwell L. Age-related changes of the corneal endothelium and stroma as seen in vivo by specular microscop y. Eye. 1987;1:197.

Skuta G, Sugar J, and Erickson E. Corneal endothelial cell measurements in megalcornea. Am J Ophthalmol. 1983;101:51.

Smolin G, Thoft RA, Dohlman CH: Endothelial function. In: The Cornea: Scientific Foundations and Clinical Practice. 3rd ed. Lippincott William & Wilkins; 1994:635-643.

Snell RS, Lemp MA (1989) Clinical Anatomy of the Eye. Mass: Blackwell Scientific Publications Inc.: 119-194.

Solomon KV, Stark WJ, Smith P: epithelial, fibrous and endothelial proliferation. St. Louis. MO. CV. Mosby. 1996; 1326-61.

Sturrock G, Sherrard E, Rice N. Specular microscopy of the corneal endothelium. Br J Ophthalmol. 1978;62:809.

-T-

Takahashi N, Sasaki K, Nakaizumi H, and Koniski F. Specular microscopic findings of lattice corneal dystrophy. Int Ophthalmol. 1987;10:47.

Thijssel MJ, Mol MJ, Timer MR: Acoustic parameters of ocular tissues. Ultrasonic Med Biol 1983; 11: 157-61.

Thomas M Aaberg, Jr, MD, Rhonda G Waldron, B-Scan Ocular Ultrasound eMedicine ,Ophthalmology, eMedicine.com. Inc. , section 3,2005.

Toth CA, Birngruber R, Boppart SA, Hee MR, Fujimoto JG, DiCarlo CD, Swanson EA, Cain CP, Narayan DG, Noojin GD, Roach WP (1997) Argon laser retinal lesions evaluated in vivo by optical coherence tomography. Am J Ophthalmol 123:188-198.

Trokel SL, Srinirasan R, Braren R: Excimer Laser surgery of the cornea Am J Ophthalmology 1983; 96:710.

Tuft SJ and Watson PG: progression of scleral disease. Ophthalmology. 1991; 98: 467-71.

-U-

Ueda Y, Duncan MK, David LL. Lens proteomics: the accumulation of crystallin modifications in the mouse lens with age. Invest Ophth Vis Sci 2002; 43(1): 205-215.

Ursea R, Colmann J, Silverman RH: Correlation of high frequency ultrasound backscatter with tumour microstructure in iris melanoma. Ophthalmology 1998; 105:906-12.

-W-

Wada I: UBM corneal thickness measurement for corneal thickness mapping. Jpn. J.Ophthalmol. 1997; 1:12-18.

Wang Z, Chen J, Yang B: Posterior corneal surface topographic changes after laser in situ keratomileusis are related to residual corneal bed thickness. Ophthalmology 1999 Feb; 106(2): 406-9; discussion 409-10.

Watson PJ and Bovey E: anterior segment fluorecein angiography. Ophthalmology 1985; 92:1-11.

Wheeler NC, Morantis CM, Kristensen RM: Reliability coefficients of three corneal pachymetries. Am J Ophthalmology 1992; 113: 645-651.

Wilkins JR, Puliafito CA, Hee MR, Duker JS, Reichel E, Coker JG, Schuman JS, Swanson EA, Fujimoto JG (1996) Characterization of epiretinal membranes using optical coherence tomography. Ophthalmology 103:2142-2151.

Wilson SE, Klyce SD. Advances in the analysis of corneal topography. Surv Ophthalmol 1991;**35**:269-277.

Woo EK, Pavlin CJ, Slomovic A: UBM quantitative analysis of light dark changes with papillary block . Am J Ophthalmology 1999;27: 43-47.

-Y-

Yanoff M and Duker JS: Ophthalmology. Mosby international Ltd.1999.

Yaylali V, Kaufman SC, Thompson HW. Corneal thickness measurements with the Orbscan topography system and ultrasonic pachymetry. J Cataract Refract Surg 1997;**23**:1345-1350.

الملخص العربي

تتطور الوسائل الحديثة لتصوير الجزء الأمامي من العين تطوراً سريعاً. و من هذه الوسائل الحديثة: المصباح الشقِي و تضاريس القرنية وعد خلايا الغشاء المبطن للقرنية و الماسح المقطعي للجزء الأمامي من العين و المجهري الحيوي الفوق صوتي و الفلوروسين المضياء.

المصباح الشقي هو ميكروسكوب خاص ثلاثي الأبعاد ويساعد علي تكبير صورة الأجزاء المختلفة من العين. وحديثاً تم إضافة كاميرا فيديو للمصباح الشقي لتصوير الجزء الأمامي من العين.

تضاريس القرنية هي طريقة لقياس وتقدير شكل وتحدب القرنية و هذه الطريقة تتقدم سريعاً بسبب التقدم الحديث في عمليات تصحيح الإبصار.

ميكروسكوب عد خلايا الغشاء المبطن للقرنية هو اختبار تصويري لرؤية الغشاء المبطن للعين وهناك نوعان من هذا الميكروسكوب: الميكروسكوب اللاصق و الغير لاصق ولتحديد كثافة الغشاء المبطن يمكن استخدام النوعان بالتبادل.

الفلوروسين المضياء هو من الوسائل الأكثر شيوعاً من خلال تعديل جهاز المصباح الشقي للتصوير. هذه الطريقة محددة لتصوير الجزء الأمامي من العين: القرنية و عدسة العين.

المجهري الحيوي الفوق صوتي يستخدم في تصوير طبقات القرنية. الوصلة بين القرنية والملتحمة يمكن ظهورها بوضوح بهذا الجهاز. جزء من الملتحمة يمكن اعتباره كنقطة هامة لقياس زاوية الحجرة الأمامية للعين باستخدام هذا الجهاز. أما القزحية فتصور جيداً بشكل مقطعي بهذا الجهاز.

الماسح المقطعي للجزء الأمامي من العين يساعد علي إعطاء تصوير دقيق في الأنسجة الحيوية بشكل مقطعي باستخدام الضوء. هو تقنية تصوير الغير ملتصق للأجزاء الشفافة. يمتاز بأنه غير ملتصق مريح يمكن للمريض أن يتحمله بسهولة.